

Population synthesis of double neutron stars.

S. Osłowski^{1,2*} and T. Bulik^{3,4} and D. Gondek-Rosińska^{4,5,6} and K. Belczyński^{3,7}

¹*Swinburne University of Technology, Centre for Astrophysics and Supercomputing, Mail H39, PO Box 218, VIC 3122, Australia*

²*CSIRO Astronomy and Space Sciences, Australia Telescope National Facility, P.O. Box 76, Epping, NSW 1710, Australia*

³*Astronomical Observatory, University of Warsaw, Aleje Ujazdowskie 4, 00-478, Warsaw, Poland*

⁴*Nicolaus Copernicus Astronomical Centre, Bartycka 18, 00716 Warszawa, Poland*

⁵*Institute of Astronomy, University of Zielona Góra, Lubuska 2, 65-265 Zielona Góra, Poland*

⁶*LUTH, Observatoire de Paris, Université Paris 7, Place Jules Janssen, 92195 Meudon Cedex, France*

⁷*Dept. of Physics and Astronomy, University of Texas, Brownsville, TX 78520, USA*

Accepted . Received ; in original form

ABSTRACT

Using the STARTRACK binary population synthesis code we model the population of double neutron stars in the Galaxy. We include a detailed treatment of the spin evolution of each pulsar due to processes such as spin-down and spin-up during accretion events as well as magnetic field decay. We also model the spatial distribution of double neutron stars by including their natal kicks and subsequent propagation in the Galactic gravitational potential. This synthetic pulsar population is compared to the observed sample of double neutron stars taking into account the selection effects of detection in the radio band, to determine the most likely evolutionary parameters. With these parameters we determine the properties of the double neutron star binaries detectable in gravitational waves by the high frequency interferometers LIGO and VIRGO. In particular, we discuss the distributions of chirp masses and mass ratios in samples selected by their radio or gravitational wave emission.

Key words: binaries: general – stars: neutron – stars: statistics.

1 INTRODUCTION

Double neutron stars (DNSs) are remarkable objects in astrophysics and their studies uniquely contribute to a number of areas of fundamental significance. The monitoring of PSR 1913+16 provided strong limits on the General Theory of Relativity (Hulse & Taylor 1975). The recent discovery of the first system with two observable pulsars J0737-3039 (Burgay et al. (2003) and Lyne et al. (2004)) has been a breakthrough in pulsar studies. The eclipses in this system provide insight in the physics of the magnetosphere (Lyutikov & Thompson 2005). Measuring the moment of inertia of pulsar A in this system would lead to a very strong constraint on the neutron star equation of state. By studying the properties of DNSs, we infer that a population of merging binaries exists. Other compact object binaries do not provide evidence of sources of gravitational waves potentially detectable by the LIGO and VIRGO observatories (Abramovici et al. (1992) and Bradaschia et al. (1991)). The origin of DNSs was first conjectured by Flannery & van den Heuvel (1975) in the context of the the Hulse Taylor pulsar

PSR 1913+16. The birth rate and properties of DNSs were investigated by Piran (1992), and by Arzoumanian et al. (1999). Belczyński & Kalogera (2001) pointed out that there may exist a large population of ultra-compact DNS binaries formed with an additional common envelope stage, and not detectable in the radio. The existence of this population relies strongly on the result of the common envelope phase with a star on the Hertzsprung gap. For a review on binary pulsars see Lorimer (2008).

Pulsar evolution was first investigated by Gunn & Ostriker (1970) soon after the discovery of pulsars. Since then, most papers concentrated on modelling the observed sample of pulsars by including all selection effects and modelling pulsar evolutionary parameters such as initial distributions, magnetic field decay, evolution of inclination, etc. (Large (1971), Taylor & Manchester (1977), Lyne et al. (1985), Stollman (1987), Emmering & Chevalier (1989), Bhattacharya et al. (1992), Hartman et al. (1997), Kalogera et al. (2001) Arzoumanian et al. (2002), Gonthier et al. (2002), Gonthier et al. (2004), Faucher-Giguère & Kaspi (2006)). These efforts concentrate primarily on classical pulsars; more recently Story et al. (2007) present models of the population of recycled millisecond pulsars. Kiel et al. (2008);

* E-mail: soslowski@astro.swin.edu.au

Kiel & Hurley (2009) are the first to take into account the effects of binary evolution leading to formation of these objects but assume initial injected distributions of magnetic fields and spin periods. Our work focuses on DNSs only and is based on different stellar evolution codes. We address the issue of pulsar populations detectable either in the radio or gravitational waves.

The evolution of binaries leading to formation of double compact objects has been investigated by many authors (Gnusareva & Lipunov 1985; Brandt & Podsiadlowski 1995; Jorgensen et al. 1995; Lipunov et al. 1995; Portegies Zwart & Yungelson 1998; Popov et al. 2000; Dewi et al. 2005; Bogomazov et al. 2005; Dewi et al. 2006; Kiel et al. 2008). Here we will be using the Star Track binary population synthesis code which was presented and used in a series of papers by Belczynski and collaborators (see Belczynski et al. (2002), Belczynski et al. (2008) and references therein). The code has been used to investigate the possible binary progenitors of gamma ray bursts and to study the rates and properties of binary gravitational wave sources (Bulik & Belczyński 2003; Bulik et al. 2004). Bulik et al. (2004) and Gondek-Rosińska et al. (2007) presented a calculation of the expected mass spectrum of merging compact object binaries including double neutron stars. They hinted at a possibility of detecting a large number of non equal mass DNS binaries, and showed that they may not show up in the radio sample due to selection effects.

In this paper we present the merger of binary population synthesis and pulsar evolution models. After applying radio selection effects we compare the predictions with the available data. The main differences between our work and that of Kiel et al. (2008) is that we base our modelling on different stellar evolution codes, focus on DNSs only and choose different field decay timescales. In Section 2 we present our model of binary evolution and pulsar evolution. Section 3 contains the results and comparison with the observations. Section 4 focuses on the mass distribution of NS visible in the radio and gravitational waves, while Section 5 contains the conclusions.

1.1 Properties of known double neutron star systems

Currently there are ten known pulsars in nine DNS binaries. In one case, both stars in the binary have been observed as radio pulsars (J0737-3039), but the B pulsar is no longer visible due to the spin precession and expected to reappear in the year 2035 (Perera et al. 2010). The spin period versus spin period derivative diagram ($P - \dot{P}$) for these binaries is presented in Fig. 1. Most of the objects are concentrated in the region of the partially recycled pulsars. However, there are two noticeable outliers: J0737-3039B, the companion of the J0737-3039A; and J1906-0746, a young pulsar likely to have a neutron star companion. The pulsar B2127+11C probably had a very different dynamical history. It lies within the globular cluster M15, where three body interactions could have replaced its original companion with a neutron star and have kicked the pulsar further away from the cluster’s core (Phinney & Sigurdsson 1991). Detailed properties of these systems can be found in Table 1, sorted by the time remaining to coalescence (merger times). Three binaries at the bottom of the table have merger times

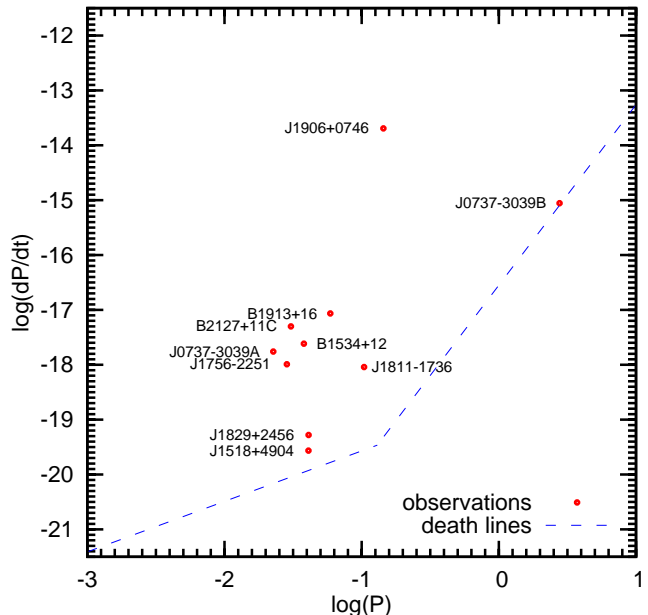


Figure 1. Observed double neutron stars on $P - \dot{P}$ diagram. Name of each pulsar is given next to it. We currently know about 10 pulsars in DNS binaries. In one case both are visible as radio pulsars (J0737-3039). The death lines are described in Section 2.3.8.

much longer than 10 Gyr. We list the spin periods and their derivatives, the masses of the neutron star, as well as the present orbital parameters. The distribution of the orbital periods spreads over two orders of magnitude, with no clear evidence of clustering in this range. The orbits of all of the systems are significantly eccentric. The masses of the seven objects with merger times shorter than 10 Gyrs are very well determined and are in the range between 1.25 and 1.44 M_{\odot} . The masses of the neutron star in the remaining three binaries are not so well constrained and may even lie outside this range.

1.2 Radio pulsars and the population observable in gravitational waves

Due to selection effects the observed sample of DNS binaries might differ from the intrinsic population. For the same reason the population observed in the radio might have different properties than the one we would observe in the gravitational waves. This has implications for the interpretation of the results from laser interferometer gravitational waves observatories.

The most obvious selection effect in the radio is the inverse square law. Our radio-telescopes have a limited sensitivity, so we will not see the weakest and/or farthest pulsars. The DNS population observed in the radio is so far restricted to our Galaxy. In this paper we model the radio selection effects due to the interstellar medium and the telescope properties (described in detail in Section 2.4). In our calculations we incorporate another selection effect which is due to the fact that the pulsars are in binaries. When searching for pulsars with stack search and phase modulation methods, it is difficult to detect radio emission from neutron stars in binaries with an orbital period shorter than 4h (Faulkner

Table 1. Properties of the observed pulsars in DNS binaries. The table contains names, spin period, spin period derivative, orbital period, mass of observed neutron star, mass of the companion, eccentricity of the orbit and time to merger. All given digits are significant. Errors, where given, are $1 - \sigma$ errors. References: 1 - Stairs (2004), 2 - Jacoby et al. (2006), 3 - Kasian (2008), 4 - Weisberg & Taylor (2005), 5 - Faulkner et al. (2005), 6 - Janssen et al. (2008).

Name	P [ms]	\dot{P} [$ss^{-1}/10^{-18}$]	P_{orb} [h]	M_{obs} [M_{\odot}]	M_{cmp} [M_{\odot}]	e	τ_{mrg} [Gyr]	Reference
J0737-3039A	22.70	1.74	2.454	$1.337^{+0.005}_{-0.005}$	$1.250^{+0.005}_{-0.005}$	0.088	0.085	1
J0737-3039B	2773	8.8×10^2	2.454	$1.250^{+0.005}_{-0.005}$	$1.337^{+0.005}_{-0.005}$	0.088	0.085	1
B2127+11C	30.53	4.99	8.05	$1.358^{+0.01}_{-0.01}$	$1.34^{+0.01}_{-0.01}$	0.681	0.2	2
J1906+0746	144.07	2.028×10^4	3.98	$1.248^{+0.018}_{-0.018}$	$1.365^{+0.018}_{-0.018}$	0.085	0.3	3
B1913+16	59.03	8.63	7.752	$1.4414^{+0.0002}_{-0.0002}$	$1.3867^{+0.0002}_{-0.0002}$	0.617	0.3	4
J1756-2251	28.46	1.02	7.67	$1.312^{+0.017}_{-0.017}$	$1.258^{+0.018}_{-0.017}$	0.181	1.7	5
B1534+12	37.90	2.43	10.098	$1.3332^{+0.001}_{-0.001}$	$1.3452^{+0.001}_{-0.001}$	0.274	2.7	1
J1811-1736	104.182	0.91	451.20	$1.62^{+0.22}_{-0.55}$	$1.11^{+0.53}_{-0.15}$	0.828	>10	1
J1518+4904	40.935	0.027	207.216	$0.72^{+0.51}_{-0.58}$	$2.00^{+0.58}_{-0.51}$	0.249	>10	6
J1829+2456	41.0098	0.05	28.0	$1.14^{+0.28}_{-0.48}$	$1.36^{+0.50}_{-0.17}$	0.139	>10	1

2004). In general, this is because the signal-to-noise ratio drops drastically due to variation of the pulsar period during the observation. This orbital period limit was calculated for a pulsar with a spin period $P = 9$ ms (Faulkner 2004), while the limit may vary as a function of P . We took this effect into account in this approximate form, but it has a very small impact on the results. Another important consequence of this effect is the reduced number of discovered binaries in pulsar surveys. In addition, there are different methods of detecting radio pulsars which are more sensitive to pulsars of such properties. The so called acceleration searches recover the signal-to-noise ratio by modelling the drift of the pulsar spin period due to its orbital motion. These methods are not always implemented in searches for new pulsars in survey data, but progress in this area is being made (e.g. Ransom et al. (2003)). In practice, the acceleration searches are often not included in the standard pipeline processing of survey data since they are very computationally expensive.

Our first aim is to investigate how the described selection effects influence the observed properties of the radio pulsar population. We model the evolution of pulsars in binaries and compare the results of different models with observations. Binaries detectable in the gravitational waves are those with a relatively small orbital separation. We assume that only binaries with a coalescence time shorter than 10^{10} years are representative of the population detectable in the gravitational waves. The strength of the gravitational wave signal during the inspiral phase depends on the chirp mass of the binary. This is the main selection effect for DNS's observability in the gravitational waves (see Section 2.5). In Bulik et al. (2004) and Gondek-Rosińska et al. (2005b) the authors suggest that there will be differences between the DNS population observable in the radio and gravitational waves. In particular, they conclude that the mass ratio distributions will not be the same for the two populations. The population modelling in those papers was based on a number of invalid assumptions. The binaries with lifetimes above the Hubble time were neglected, and it was assumed that observability of pulsars is proportional to their lifetime. The gravitational wave strains are very low and the signals that interferometric detectors are trying to detect are buried in noise. Numerical relativity calculations provide an input for statistical methods that enable the detection of a known sig-

nal from the noise. Until recently most calculations of coalescing neutron star and/or black hole binaries assumed that the mass ratio is close to unity (e.g. Gondek-Rosińska et al. (2007), Buonanno et al. (2007)). In this paper we use the results of modelling the radio selected population to obtain the mass ratio distributions of DNS systems. We check whether the pulsars potentially detectable in the gravitational waves have the same properties as the radio population.

2 DESCRIPTION OF THE MODEL

2.1 STARTRACK binary population synthesis code

In order to perform a population synthesis of double neutron stars we need to know what the population of DNS binaries itself look like. We used the STARTRACK code for this purpose (Belczynski et al. 2008). This code has been improved for many years now and is considered to be the state-of-the-art with regard to our current understanding of stellar evolution. STARTRACK has been extensively tested, calibrated and its results have been compared to observations (e.g. Belczynski et al. 2002; Belczynski & Bulik 2002; Belczynski et al. 2002, 2008). At the base of this code are analytic formulae describing the evolution of single stars first developed by Hurley et al. (2000). The code follows a sequence of evolutionary phases of stars starting at the main sequence, passing through the Hertzsprung gap, the red giant branch or the asymptotic giant branch. After its nuclear evolution the star can form a compact object (a white dwarf, a neutron star or a black hole). The supernova explosion can completely disrupt the star leaving no remnant at all. STARTRACK includes the evolution of helium stars as well. If the star that evolves first ends up as a white dwarf or a neutron star, then there is a chance a double neutron star system will be formed, provided that the binary is not disrupted during the supernova explosions. In the STARTRACK's standard model we assume a bimodal distribution of the FeNi core masses in pre-supernova stars (Weaver & Weaver & Woosley (1993), Timmes et al. (1996)). Stars with initial masses below $\sim 18 - 19 M_{\odot}$ burn carbon convectively. They form cores of $\sim 1.5 M_{\odot}$ which yield neutron stars of $1.3 M_{\odot}$. Heavier stars burn carbon radiatively and the cores are more massive $\sim 2 M_{\odot}$ (yielding neutron

stars of $1.8 M_{\odot}$). The mass of the FeNi core does not depend sensitively on the initial star mass, but is a strong function of the burning reactions within the pre-supernova star. If similar reactions are encountered over the wide initial star mass range in which neutron stars are formed (e.g. 8-18 M_{\odot}), then the majority of neutron stars are expected to have similar masses. The previously employed neutron star mass calculation was based on stellar evolutionary models that suggest an increase of final FeNi core mass with initial star mass (e.g. Weaver & Woosley (1993); or see Table 4.4 of Vanbeveren et al. (1998)). This naturally results in a wide neutron star mass spectrum.

Some poorly known details of the stellar evolution are parametrised in the STARTRACK code. Fortunately most of them do not have a significant impact on the results relevant to this work. The various models of the binary evolution in this code are described in Section 2.2.

2.2 Evolution of the binaries

We consider three variants of the binary population synthesis models. An outline for each one of them is given below.

2.2.1 Model A - standard

This model is described in detail in Belczynski et al. (2002) and updated in Belczynski et al. (2008). Here we only present the most important features. The initial mass of one of the stars is drawn from a power law $\sim M^{-2.7}$ (Scalo 1986). The mass of its companion is determined as a random fraction of the heavier (at the time of formation) star's mass drawn from a flat distribution (Kuiper 1935). The initial orbital separation distribution is flat in logarithm, while the initial eccentricity's distribution is flat. The code calculates the carbon-oxygen core mass, which will form a compact object using formulae from the already mentioned work by Hurley et al. (2000). This mass has an impact on the baryonic mass of the newly formed neutron star due to its influence on the mass of the Fe-Ni core as described in Woosley (1986), Fryer et al. (1999) and Timmes et al. (1996)

$$M_{NS}^{bar} = \begin{cases} M_{FeNi}, & M_{CO} \leq 5M_{\odot} \\ M, & M_{CO} \geq 7.6M_{\odot} \\ M_{FeNi} + f_b(M - M_{FeNi}), & \text{otherwise} \end{cases}, (1)$$

where f_b is the fall-back factor (describing the fraction of the stellar envelope that falls back after the SN), M_{FeNi} is the Fe-Ni core mass, M_{CO} is the CO core mass and M is the pre-SN mass of the star; for details see Belczynski et al. (2008). The fall-back factor is a linear function of M_{CO} , such that $f_b(M_{CO} = 5M_{\odot}) = 0$, and $f_b(M_{CO} = 7.6M_{\odot}) = 1$. In order to convert the baryonic masses to the gravitational masses a quadratic formula is used: $M_{NS}^{bar} - M_{NS} = 0.075M_{NS}^2$, where M_{NS} is the gravitational mass. Orbital parameters are affected by tidal interactions, mass loss due to stellar winds, mass transfers, and gravitational wave emission. We parametrise the fraction of the mass ($f_a = 0.5$) taking part in a stable mass transfer that is accreted by the companion; the rest is lost from the binary. Unstable mass transfers in STARTRACK (common envelope - CE) is treated with the formalism proposed by Webbink (1984) and de Kool (1990). In this model we assume $\alpha_{CE} \times \lambda = 1.0$. The neutron star can accrete some

mass during the common envelope phase. The amount of this mass is drawn from the range $[0.05M_{\odot}, 0.10M_{\odot}]$ with a flat distribution. Each supernova explosion occurs at a random place in the orbit. We take natal kicks drawn from the Hobbs et al. (2005) distribution into account, and calculate the orbit and centre of mass velocity after the explosion.

2.2.2 Model H

Model H treats the common envelope phase differently. In this case neutron stars accrete more matter by assuming the Bondi-Hoyle accretion (Bondi & Hoyle 1944) with a hypercritical accretion rate (Brown et al. 2000). It has a crucial impact both on the binary evolution (changes in orbital separation) and on the properties of the pulsar that formed first. The amount of accreted mass is roughly 10 times more than in the standard model A. This amount depends mostly on the mass ratio in the binary prior to the common envelope q_0 . The final mass is calculated using formula (Bethe & Brown 1998):

$$M_B = (q_0 + 0.7q_0^2) M_A, (2)$$

where M_B is the mass of the acceptor after the transfer and M_A is the mass of the donor before the transfer.

2.2.3 Model S

In this model we assume a different initial mass function for the newly formed neutron stars. It assumes a very simplified linear relation between M_{NS} and the mass of the iron core M_{core} from which it is formed:

$$M_{NS} = 0.35 \times M_{core} + 0.596M_{\odot}. (3)$$

The values of the parameters are such that we have neutron stars with masses from $1.1M_{\odot}$ (forming from a star with mass $8.275M_{\odot}$ on a zero age main sequence) to $2.5M_{\odot}$ (forming from a star with mass $20.88M_{\odot}$ on a zero age main sequence). The purpose of this model is to check the influence of this poorly known relation on the distribution of the masses of the double neutron stars.

2.3 Pulsar evolution model

The previous subsections describe the models of the stellar evolution and the initial masses of the neutron stars. It remains to assign each neutron star other properties such as magnetic field and spin period. These parameters are required to model the neutron stars as radio pulsars. The STARTRACK code provides details of the interaction in the binaries. We assume that all neutron stars become radio pulsars immediately after their birth. The pulsar that is born earlier can be affected by accretion of matter from its still evolving companion. These effects are modelled and described in the following paragraphs.

Before moving to the details of our model, we briefly describe the ingredients necessary to model the life and death of each pulsar. At the very beginning we assign each neutron star a set of initial parameters such as spin period, magnetic field and moment of inertia. After that, we start evolving each pulsar. We assume a dipole model for the magnetic field (Ostriker & Gunn 1969) and base the spin-rate

evolution on that. Since we only consider double neutron stars, we need to consider mass transfer and how it affects radio pulsars. During accretion the neutron stars are visible in the X-ray and not detectable in the radio. In this paper we do not model the X-ray emission as it only occurs for a short period of time compared to the radio activity periods. The evolution of binaries, along with their movement in the Galaxy, is followed until the coalescence due to gravitational wave emission or for 10 Gyr, whichever is shorter.

2.3.1 Initial parameters

Our model starts treating each neutron star as a radio pulsar immediately after its formation. The initial magnetic field is drawn from a flat logarithmic distribution in the range $10^{11} \text{G} \leq B \leq 10^{13} \text{G}$.

The initial spin period is, in most models, $P_{ini} = 10 \text{ ms}$. The choice of this parameter is not very important. Even if some (or all) of the pulsars were born with longer or shorter spin periods, the overall properties of the resulting population would not change significantly unless we vary the initial period by more than a factor of 10. As a matter of fact, longer initial periods will make it harder to get a good fit to the observations. This will be demonstrated by the model APD05I where we allow a uniform distribution of the initial spin periods between 10 and 100 ms as motivated by some observations (Faucher-Giguère & Kaspi 2006). This will make the model slightly worse as it will be harder to spin pulsars up to short enough spin periods. Young pulsars spend a very short time in the region of the $P - \dot{P}$ diagram where they are born and move quickly towards longer spin periods. Given the small number statistics of the observed sample, it is not possible to distinguish the models with more realistic P_{ini} distributions. As a consequence and for the sake of simplicity most of the models we present will have $P_{ini} = 10 \text{ ms}$ for all the pulsars. We have tested models with longer initial periods, up to 100 ms, but we found 10 ms to be the optimal initial period.

The radius $R = 10 \text{ km}$ and moment of inertia $I = 10^{45} \text{ g} \times \text{cm}^2$ are the same for all the pulsars.

As mentioned before, we consider only spin-down due to dipole emission. This yields the braking index $n = \dot{\Omega}\Omega^{-2} = 3$ and determines the spin frequency evolution. Observations show that the braking indices of pulsars are in the range $\approx 2.5 - 3.5$ (Manchester et al. 2005). Following the pulsar dipole model, the rotation of the neutron star slows down with the initial frequency time derivative:

$$\dot{\Omega} = -\frac{2B^2 R^6 \sin^2 \alpha}{3c^3 I} \Omega^3, \quad (4)$$

where α is the angle between the rotation and magnetic field axis, B is the magnetic field, R is the neutron star radius, c is the speed of light and I is the moment of inertia of the neutron star. We assume $\alpha = 30^\circ$ for each pulsar, as values of $\alpha < 45^\circ$ have been shown to provide better fits to observations (Contopoulos & Spitkovsky 2006). The magnetic field strength and the angle α are degenerate so we do not lose anything in making this assumption. This degeneracy extends to the evolution of the field and the inclination angle. At every point in the evolution, the magnetic field is given by

$$B = 6.4 \times 10^{19} \sqrt{P\dot{P}} \text{ Gauss}. \quad (5)$$

2.3.2 Evolution of the magnetic field

If there are no direct interactions between the binary members, the spin period and its evolution are independent of the companion's properties. This is the case after the formation of the first pulsar, unless there is ongoing mass accretion, and after the formation of the second neutron star until the contact of magnetospheres and coalescence. During these periods of independent evolution, constituting most of the pulsar's lifetime, the spin period evolves according to Equation 4. In addition we assume that the magnetic field of a pulsar is decaying exponentially in time via Hall-like effect with ohmic dissipation (Romani (1990); Geppert & Urpin (1994); Urpin & Geppert (1995); Urpin et al. (1997); Konar & Bhattacharya (1997, 1999a,b), see also Section 2.3.3 for other possibilities):

$$B = (B_0 - B_{min}) \cdot \exp\left(-\frac{t}{\tau_d}\right) + B_{min}, \quad (6)$$

where τ_d is the magnetic field decay timescale. The decay of the magnetic field is controversial. Some analyses show that it proceeds on a timescale of 2 – 5 Myrs (Gonthier et al. 2002, 2004), while others (Faucher-Giguère & Kaspi 2006) argue that it may be an artefact of the assumed luminosity law. Kiel et al. (2008) obtains the best model with a long (≈ 2000 Myrs) timescale for the decay of the magnetic field. In their model, the initial spin period is correlated with the initial magnetic field. Gonthier et al. (2010) have tested both possibilities and finds that it is not possible to create a good synthetic population without either quickly decaying the magnetic field or correlating the initial spin periods with the magnetic fields. This work suggests that it is easier to reproduce the observed population in the first case and our models will follow that path. The short timescale of the magnetic field decay can be interpreted as a way of modelling the deviations of the pulsar spin evolution from the standard dipole model. This is supported by the fact that there seems to be some additional torque in the pulsar evolution (Faucher-Giguère & Kaspi 2006). The caveat of this solution is that the second neutron star can pass through the region of the partially recycled pulsars without accreting any mass. However the fraction of the recycled pulsar's contribution to that region is high and they dominate the results for most of the models (see Section 3.2). While the main goal of this work is to look for differences between the populations visible in the radio and potentially detectable by gravitational wave detectors we also attempt to distinguish between different physical models of the magnetic field evolution and to create an improved model of the pulsar spin-down. We want our modelled pulsars to evolve as described by the standard dipole model at later stages of their life; therefore we assume that after the first born pulsar accretes any amount of mass its field ceases to decay. The models with very long timescale decays of 1 Gyr and more are an exception to that rule. In these cases the magnetic field decays for the whole lifetime of the pulsar. In addition, Zhang & Kojima (2006) shows that there is a lower limit to the magnetic field strength. We adopt their value of $B_{min} = 10^8 \text{ G}$. The magnetic field decay ceases once the field reaches this value.

2.3.3 Roche lobe overflow

Before the second supernova explosion occurs, the companion of an already formed pulsar continues its stellar nuclear evolution. If it fills its Roche lobe during this period, then mass transfer onto the pulsar can occur and the system becomes an X-ray binary. Some of the mass from the system is lost and the rest is accreted onto the neutron star. In addition to increasing the mass of the neutron star this has three effects:

(I) we assume that the magnetic field decays. The physical process explaining this quenching might be the aforementioned ohmic dissipation (changes of the crust's resistance due to heating during accretion). Other groups consider the magnetic field burial as another possible cause of the accretion-induced field decay (Bisnovatyi-Kogan & Komberg 1974; Taam & van den Heuvel 1986; Melatos & Phinney 2001; Cumming et al. 2001; Choudhuri & Konar 2002; Konar & Choudhuri 2004; Lovelace et al. 2005). Another option is tying the evolution of the magnetic field to changes in the pulsar spin period through the vortex-fluxoid interactions. The proton vortices which carry the magnetic field are dragged by the neutron vortices inwards or outwards in the radial direction when the pulsar is spun-up or spun-down, respectively (Muslimov & Tsygan 1985; Ruderman 1991a,c,b; Jahan-Miri 2000). We generally favour the ohmic dissipation as we adopt an exponential decay. However we do not try to distinguish between the three possibilities and only note that the vortex-fluxoid interactions would have consequences for our propeller modelling as it depends on the spin change (see 2.3.6). We model the magnetic field change as:

$$B = (B_0 - B_{min}) \cdot \exp\left(-\frac{dM}{\Delta M_d}\right) + B_{min}, \quad (7)$$

where dM is the accreted mass and ΔM_d is magnetic field decay mass scale, and B_{min} is the minimal magnetic field of a neutron star. This approach is similar to the one adopted by Kiel et al. (2008). Other possibilities based on the observed correlation between the magnetic field and the estimated accreted mass for binary X-ray sources have also been explored by Shibazaki et al. (1989). However, their formula gives very similar results in the relevant range of accreted mass. After the mass accretion induced decay, the field stops to decrease in time, i.e. it is fixed at the final level unless another mass transfer will happen. In the latter case the field decays in the same way as in the first event. The lower limit for the magnetic field still applies with $B_{min} = 10^8$ G.

(II) the pulsar in the accretion phase does not emit in the radio. This is because the magnetosphere is filled by the accreted gas, and the particle acceleration is not effective. The pulsar is visible in the X-ray band, but in this work we do not model this. During the accretion pulsars will not contribute to our radio detectable population.

(III) the spin period of a pulsar is affected. Due to angular momentum transfer the neutron star tends to corotate with the accreted matter at the Alfvén radius:

$$R_A = \left(\frac{8R^{12}B^4}{M\dot{M}^2G}\right)^{\frac{1}{7}}. \quad (8)$$

The accretion rate \dot{M} is calculated within the STARTRACK code by considering the detailed evolution of the companion

(Belczynski et al. 2008). The orbital velocity at Alfvén radius equals:

$$\Omega_A = \sqrt{\frac{GM}{R_A^3}}. \quad (9)$$

Following the accretion, the pulsar will spin with the angular velocity $\Omega_f = \Omega_A$, where Ω_f is the final velocity after the mass transfer. Depending on the model, it might exhibit different behaviour, as described in 2.3.4 and 2.3.6.

2.3.4 Partial spin-up

If the amount of accreted matter during the Roche lobe overflow (see 2.3.3) is sufficient, namely $dM \geq 0.1M_\odot$, we then assume that the pulsar will be spun up fully to the orbital frequency of the material at the Alfvén radius Ω_A . Note that if the matter at the Alfvén radius has an angular velocity smaller than the neutron star has, it can spin down the neutron star. This is happening via the propeller effect (see 2.3.6). If the accreted mass is smaller than $0.1M_\odot$ then the pulsar can be only spun-up to a fraction of Ω_A . We assume that the amount of angular momentum transferred is proportional to the accreted mass:

$$\Delta J \propto \frac{dM}{0.1M_\odot}, \quad (10)$$

This assumption yields a linear relationship between the amount of the accreted mass and the final angular velocity of the pulsar:

$$\Omega_f = \Omega_0 + (\Omega_A - \Omega_0) \frac{dM}{0.1M_\odot}, \quad (11)$$

where Ω_f is the final angular velocity, Ω_A is the angular velocity at the Alfvén radius and Ω_0 is the initial angular velocity before recycling.

2.3.5 Common envelope

The formation of double neutron stars involves quite frequently an unstable mass transfer, i.e. a common envelope phase. During the common envelope phase the binary orbit is tightened, and a significant amount of matter from the companion is expelled. At the same time some matter is accreted onto the neutron star, see Section 2.2.1 and references therein. In the STARTRACK code the common envelope is treated following the Webbink (1984) formalism and assuming that the amount of matter accreted by the neutron star lies in the range $0.05M_\odot \leq dM \leq 0.10M_\odot$, randomly drawn from it with a flat distribution. The duration of the common envelope phase is highly uncertain, but accretion of such an amount of matter would correspond to a highly super-Eddington accretion rate. At this stage the angular momentum transfer is chaotic (Benensohn et al. 1997), and we assume that the spin of the neutron star is not affected on the average by accretion during this phase, i.e. the spin period of the pulsar is the same as before the common envelope. However, the accreted matter quenches the magnetic field of the neutron star, according to Equation (7). Thus, a system after a common envelope phase has a tightened orbit, and the pulsar is more massive with a decreased magnetic field yet its spin frequency is unchanged. Another possibility is that there is no accretion of matter onto the neutron

star in that phase. In these models the pulsars mainly evolve along the field decay lines, which does not yield a good fit to the observed population (see Section 3.2).

2.3.6 The propeller effect

Here we consider the case of a pulsar rotating with a greater velocity than the matter orbiting at the Alfvén radius. Illarionov & Sunyaev (1975) suggested that in this case the propeller effect takes place: the centrifugal force at the Alfvén radius is pushing the matter away, inhibiting the accretion onto the neutron star, assuming that most of the mass in the disc is ejected from the system. X-ray observations support the propeller effect (e.g. Cui (1997)).

In Section 2.3.3 we describe how accretion can spin up or down the neutron star. This propeller mechanism is responsible for spinning down the neutron star. However, there has been recent suggestions that the propeller effect might be ineffective at low accretion rates (Romanova et al. 2004; D’Angelo & Spruit 2010). The mass cannot be completely ejected from the system and piles up at the edge of the disc. After some time the pressure will overcome the centrifugal barrier and the accretion will proceed. This happens quasi-periodically. We consider the possibility that the mass can be accreted in the end and that the magnetic field is quenched during the quasi-periodic accretion events which have no net effect on the pulsar’s spin period. Our motivation for including this approach is that we need to be able to reduce the pulsar’s magnetic field without affecting its spin period in order to get a good fit to observations. Models with this ineffective propeller treatment are noted with the letter P.

In the remaining models we allow the propeller effect to take place and the neutron star to be both spun down or up. The outcome depends on the value of the magnetic field and the accretion rate.

2.3.7 Evolution of the orbit

When both pulsars are formed and there is no more mass exchange between the two neutron stars, the only change in the orbit can be attributed to the emission of gravitational waves. This effect is very weak in general, but the tight binaries will be strongly influenced by the emission of the gravitational waves. We calculate the corresponding evolution of the orbit in the first post-Newtonian approximation. The time derivatives of the eccentricity and the semi-major axis are (Peters 1964):

$$\frac{da}{dt} = -\frac{64}{5} \frac{G^3 (M_1 + M_2)^2}{c^5 a^3 (1 - e^2)^{\frac{7}{2}}} \left[1 + e^2 \left(\frac{73}{24} + \frac{37}{96} e^2 \right) \right], \quad (12)$$

$$\frac{de}{dt} = -\frac{304}{5} e \frac{G^3 (M_1 + M_2)^2}{c^5 a^4 (1 - e^2)^{\frac{5}{2}}} \left(1 + \frac{121}{304} e^2 \right). \quad (13)$$

The evolution of the orbit is taken into account for the entire evolution of the binary, which is until they coalesce, unless it takes more than 10 Gyr.

The pulsars can be radio loud (see 2.3.8) until the magnetospheres join. This is when the semi-major axis of the system is smaller than the sum of light cylinder radii:

$$a < \frac{c}{2} \left(\frac{1}{\Omega_1} + \frac{1}{\Omega_2} \right), \quad (14)$$

where a is the semi-major axis, c is the speed of light, Ω_1 and Ω_2 are angular velocities of the first and second pulsar respectively. The magnetospheres touch in practice always at the same numerical step as the coalescence of the pulsars. This means that they can be radio loud until the very end.

2.3.8 Radio luminosity

In order to check the influence of the selection effects and compare the populations visible in the gravitational waves and in the radio, we need to know the radio luminosity of all the pulsars. We use the Narayan & Ostriker (1990) model fitted to the observations, also used by Hartman et al. (1997):

$$\log_{10} L_{400} = \frac{1}{3} \log_{10} \left(\frac{\dot{P}_{-15}}{P^3} \right) + 1.635, \quad (15)$$

where $P_{-15} = \frac{\dot{P}}{10^{-15}}$. This luminosity is given in units of $mJy \times kpc^2$ for observations at 400 MHz.

Even now, with the bigger sample of pulsars this model provides a reasonably good description of the observed luminosities when compared to the Australia Telescope National Facility pulsar catalogue¹ (Manchester et al. 2005). Although the spread in the observed luminosities is clearly visible, the luminosities are clustered around the modelled values. However selection effects can affect the observed luminosity model, so the observed luminosities should be compared to a model after taking the selection effects into account.

An alternative luminosity model has been derived by Faucher-Giguère & Kaspi (2006). This model is able to explain the lack of the pile-up of pulsars near the death lines without invoking the decay of magnetic field. The comparison sample used by Faucher-Giguère & Kaspi (2006) is very different from our sample. The known DNS systems contain mainly mildly recycled pulsars. At the same time the luminosity model from Faucher-Giguère & Kaspi (2006) is biased towards millisecond pulsars. The observed DNS population does not contain such objects, so any luminosity model favouring these pulsars will be found less likely in our likelihood analysis (see Section 3.2). The choice of luminosity function is connected to the field decay timescale (see the discussion in Section 2.3.3). For comparison, we present one model with the luminosity function used by Faucher-Giguère & Kaspi (2006):

$$\log_{10} L_{1400} = \log_{10} (L_0 P^{-1.5} P_{15}^{0.5}) + L_{corr}, \quad (16)$$

where L_{1400} is the luminosity at 1400 MHz, $L_0 = 0.18 \text{ mJy} \times kpc^2$ is the scaling factor and L_{corr} is randomly chosen from zero-centred normal distribution with standard deviation $\sigma_{L_{corr}} = 0.8$.

The pulsars cease to emit in the radio once they cross the so-called death lines. After crossing these lines on the $P - \dot{P}$ diagram the pulsar’s emission mechanism fails as electron-positron pairs can no longer be created in the magnetic field. In this work we assume that all the pulsars cease their emission after crossing the two death lines defined by (Rudak & Ritter 1994):

$$\log_{10} \dot{P} = 3.29 \times \log_{10} P - 16.55, \quad (17)$$

¹ <http://www.atnf.csiro.au/research/pulsar/psrcat>

Table 2. Free parameters in the evolution model

Parameter	Default value
τ_d	5 Myr
ΔM_d	$0.025 M_\odot$
B_0	$[10^{11} \text{ G}, 10^{13} \text{ G}]$
B_{min}	10^8 G
I	$10^{45} \text{ g} \times \text{cm}^2$
R	10 km
α	30°
ΔM_{min}	$0.1 M_\odot$

τ_d is the timescale of field decay, ΔM_d is the mass scale of field decay, B_0 is the initial magnetic field, B_{min} is the minimal magnetic field, I is the moment of inertia, R is the pulsar radius, α is the angle between rotation and magnetic axis, while ΔM_{min} is the accreted mass limit for full spin-up.

$$\log_{10} \dot{P} = 0.92 \times \log_{10} P - 18.65. \quad (18)$$

These relations are empirical. Although there are cases known in which a pulsar is found beyond these death lines (Young et al. 1999), they describe the cut-offs on the P - \dot{P} diagram quite well. None of the DNS systems is found to be beyond the death lines we adopt here.

For the discussion of the implemented radio selection effects we refer the reader to Section 2.4.

2.3.9 Numerical step size

In order to choose the length of the numerical step size during the evolution of a DNS we calculate the number of time derivatives describing the rate of change of pulsar properties. The step is chosen to satisfy the following conditions: (i) the pulsar period changes by less than 1% (ii) the semi-major axis of the orbit changes by less than 1%, (iii) the step is limited by the beginning of the next mass transfer episode, (iv) the time step is shorter than 1 Gyr. The last condition was introduced to follow the evolution of mildly recycled millisecond pulsars with a weak field on wide orbits.

2.3.10 Free parameters

We list the parameters describing the evolution of the pulsars in Table 2. The values of the evolutionary parameters for the several considered models are given in Table 3. The models are denoted as follows: the first letter in the name of model refers to the stellar evolution model in the STARTRACK code; the letter P means that the model incorporates the inefficient propeller effect. The letter F implies that full spin-up is always possible in the given model. In other words, all the pulsars are recycled to the orbital velocity at Alfvén radius regardless of the amount of accreted matter; the letter D followed by a number refers to the magnetic field decay mass scale ΔM_d . The letter C means that there is no accretion in the CE phase. The letter I stands for a different assumption about the initial spin periods, see Section 2.3.1. The letter L is used for models with a different radio luminosity prescription, see Section 2.3.8. Finally, the letter T followed by a number gives the value of the magnetic field decay timescale in Myrs. In the case of T1k and T2k (time decay timescale of 1 and 2 Gyrs) it also means

that the magnetic field decays for the lifetime of the pulsar - the quenching does not stop after an accretion event.

2.3.11 Motion in the Galaxy

In order to calculate the observed radio fluxes of our pulsar population we need to model their motion in the Milky Way. Therefore we consider a simple model of the Galaxy consisting of the following three components: a bulge, a disk, and a halo. The bulge and disk potential are described by the Miyamoto & Nagai (1975) type potential, also used by Paczynski (1990); Bulik et al. (1999):

$$\Phi(r, z) = \frac{GM}{\sqrt{R^2 + (a + \sqrt{z^2 + b^2})^2}}, \quad (19)$$

where M is the total mass of a given component, $R = \sqrt{x^2 + y^2}$, and a, b are the free parameters. The halo is described by the density distribution $\rho = \rho_c [1 + (r/r_c)^2]^{-1}$ with a cut-off at $r_{cut} = 100 \text{ kpc}$ above which the halo density is zero. The corresponding potential for $r < r_{cut}$ is

$$\Phi(r) = -\frac{GM_h}{r_c} \left[\frac{1}{2} \ln \left(1 + \frac{r^2}{r_c^2} \right) + \frac{r_c}{r} \arctan \left(\frac{r}{r_c} \right) \right]. \quad (20)$$

We use the following values of the parameters (Blaes & Rajagopal 1991) describing the bulge (index 1) and disk (index 2) potential: $a_1 = 0 \text{ kpc}$, $b_1 = 0.277 \text{ kpc}$, $a_2 = 4.2 \text{ kpc}$, $b_2 = 0.198 \text{ kpc}$, $M_1 = 1.12 \times 10^{10} M_\odot$, $M_2 = 8.78 \times 10^{10} M_\odot$, while for the halo potential we use $M_h = 5.0 \times 10^{10} M_\odot$, and $r_c = 6.0 \text{ kpc}$. The distribution of stars in the disk is assumed to be that of a young disc (Paczynski 1990). The radial and vertical distributions are independent i.e. the distributions factor out:

$$P(R, z) \propto R(R) dR p(z) dz, \quad (21)$$

where the radial distribution is $p(R) \propto \exp(-R/R_{exp})$, and $R_{exp} = 4.5 \text{ kpc}$, and we introduce an upper cut-off at $R_{max} = 20 \text{ kpc}$. The vertical distribution is exponential $p(z) \propto \exp(-z/75 \text{ pc})$.

We distribute our modelled binaries in the Galaxy by choosing their location randomly to mimic the densities described above. The velocity of the binary corresponds to its location in the Galaxy. We also give both neutron stars natal kicks, as obtained from the STARTRACK. We use the leapfrog method in the KDK (kick-drift-kick) scheme with a constant (10^5 years) time step. This approach is fully symplectic. In other words, it is equivalent to solving the Hamilton's equations of motion and fully preserves energy and angular momentum (e.g. Quinn et al. (2010)).

2.4 Detection in the radio band

We use the radiometer equation (Dewey et al. 1985) to calculate the minimum flux necessary to detect the pulsar for a given signal-to-noise (S/N) threshold:

$$S_{min} = \beta \frac{(S/N_{min})(T_{rec} + T_{sky})}{G \sqrt{n_{pt} t_{int} \Delta f}} \sqrt{\frac{W_e}{P - W_e}}, \quad (22)$$

where β is a parameter arising from digitisation errors (e.g. $\beta = 1.25$ for one bit digitisers) and other effects reducing the S/N, such as radio frequency interference or distortion of the bandpass, T_{rec} is the receiver noise temperature, T_{sky}

Table 3. Models of pulsar evolution. The last column describes what is changed in the model with respect to the standard possibilities, including initial period variation in range 10 to 100 ms, no accretion in the CE phase, a different luminosity law and a continuous decay of magnetic field.

Model	τ_d	ΔM_d	propeller	spin-up	STARTRACK model	other
A	5	0.025	yes	partial possible	A	-
AF	5	0.025	yes	always full	A	-
APD05	5	0.05	inefficient	partial possible	A	-
APD05L	5	0.025	inefficient	always full	A	luminosity
APD05I	5	0.05	inefficient	partial possible	A	initial period
APD05T1k	1000	0.05	inefficient	partial possible	A	magnetic field
APD003T2k	2000	0.0033	inefficient	partial possible	A	magnetic field
AP	5	0.025	inefficient	partial possible	A	-
APC	5	0.025	inefficient	partial possible	A	no CE
APT20	20	0.025	inefficient	partial possible	A	-
HP	5	0.025	inefficient	partial possible	H	-
SP	5	0.025	inefficient	partial possible	S	-

is the sky temperature in the direction of given pulsar, G is the antenna gain, n_p is the number of polarisations, t_{int} is integration time, Δf is the receiver bandwidth, W is the pulse width and P is the pulsar period (Lorimer & Kramer 2004). The first part of Equation 22 is the usual radiometer equation, while the second part (the square root) is the pulsar term. We will assume that $\beta = 1$. Other values required to calculate the minimum flux for the pulsar’s detection are taken to mimic the most successful pulsar survey, the Parkes Multibeam Pulsar Survey (e.g. Manchester et al. (2001)).

We have taken into account the broadening of the pulse width due to the distribution of electrons in the Galaxy (Cordes & Lazio 2002), interstellar scattering and sampling time of a survey, so that the effective width of the pulse entering Equation (22) is (e.g. Burgay et al. (2006)):

$$W_e^2 = W_i^2 + \tau_{samp}^2 + \left(\tau_{samp} \cdot \frac{DM}{DM_0} \right)^2 + \tau_{scatt}^2, \quad (23)$$

where W_i is the intrinsic pulse width, τ_{samp} is the survey sampling time, DM is the dispersion measure in the direction of the pulsar, DM_0 is the diagonal dispersion measure of the survey and τ_{scatt} is the interstellar scattering time. Bhat et al. (2004) have obtained a fit of τ_{scatt} as a function of the dispersion measure and this model is used in this paper. We assume that all the pulsars have the duty cycle $\frac{W_i}{P} = 0.05$. Observations show that there is a dependence of the duty cycle on the pulsar’s period (e.g. Lyne & Manchester (1988)), but we neglect that for simplicity. Effective widths, dispersion measures and S_{min} are calculated with a modified version of the PSREVOLVE² code written at the Centre for Astrophysics and Supercomputing, Swinburne University of Technology.

To calculate the limiting flux density we choose a realistic signal-to-noise detection threshold of $(S/N_{min}) \geq 10$. We then compare S_{min} with our modelled luminosity of all the radio loud pulsars. If the observed flux exceeds this limit we assume that this pulsar is detectable in the radio.

While calculating the properties of the radio population, we model the beam width of the pulsar as a function

of its spin period. We adopt the results of Tauris & Manchester (1998) and assume that the beaming fraction is:

$$f_{beaming} = 9 \left(\log \frac{P}{10} \right)^2 + 3, \quad (24)$$

where P is the rotational period of the pulsar in seconds. This formula has been obtained by fitting to slow rotating pulsars and is a good fit for pulsars with $P \gtrsim 100ms$.

Since the radio luminosity model described in 2.3.8 provides the radio luminosity at 400 MHz, we need to translate these values into luminosities at 1420 MHz, as this is the frequency used by the Parkes Multibeam Pulsar Survey:

$$L_{1420} = L_{400}^{\alpha_{sp}}, \quad (25)$$

where L_{1420} is the luminosity at 1420 MHz, L_{400} is the luminosity at 400 MHz calculated from Equation 15, and α_{sp} is the spectral index. We adopt the $\alpha_{sp} = -1.8$ value from Maron et al. (2000)

2.5 Detection in gravitational waves

The gravitational wave detectors such as LIGO and VIRGO, (for sensitivity estimates see: (Flanagan & Hughes 1998) and (Kulczycki et al. 2006)) are currently working and in principle can detect neutron star coalescence with a chirp mass of $1.2 M_{\odot}$ as far as 18 Mpc. The signal-to-noise ratio from the inspiral phase of two compact objects is given by

$$\frac{S}{N} \sim M_{chirp}^{\frac{5}{6}} \times \frac{1}{D}, \quad (26)$$

where D is the distance from the observer and $M_{chirp} = (M_1 M_2)^{0.6} (M_1 + M_2)^{-0.2}$ is the chirp mass, where M_1 and M_2 are the masses of the first and second star in the system respectively. We define the DNS population observable in the gravitational waves as consisting of binaries with merger time shorter than the Hubble time. All the observable quantities of the DNSs are weighted by the volume in which they are observable, i.e.:

$$V \sim M_{chirp}^{\frac{5}{2}}. \quad (27)$$

Thus the gravitational wave population is the population residing in multiple galaxies and we assume that the populations in these galaxies resemble the one in our Galaxy. We

² <http://astronomy.swin.edu.au/~fdonea/psrevolve.html>

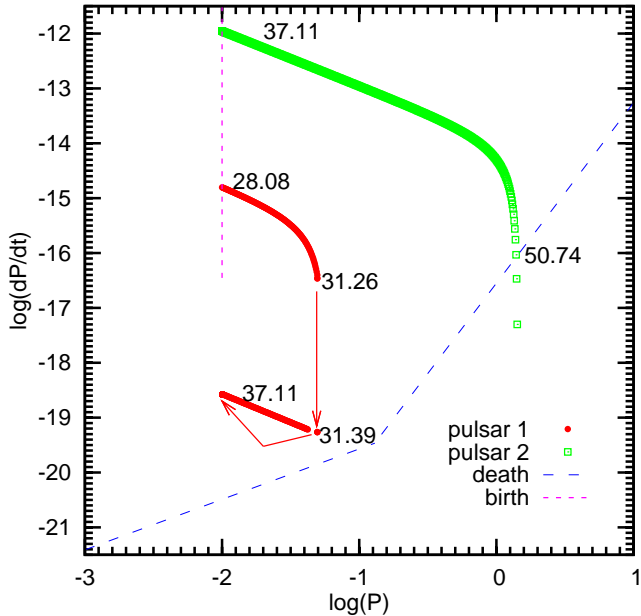


Figure 2. An example of a neutron star binary evolution on the $P - \dot{P}$ diagram. The dotted line corresponds to the birth line, where all neutron stars are formed in our model. The solid lines represent the death lines. The numbers correspond to characteristic ages in Myrs and are explained in the text (Section 3.1). Arrows show how the mass transfer affects the first pulsar.

neglect a possible detection of gravitational waves in the merger and the ringdown phases of the coalescence.

3 RESULTS

3.1 Example of a binary evolution

In subsection 2.3 we described our phenomenological model of pulsar evolution. In Fig. 2 we present an example of an evolutionary path for one of the simulated binaries. This example is based on the AF model, founded on the STARTRACK model A with full spin regardless of the total accreted mass.

The pulsars are born with a rotational period $P_{ini} = 10$ ms at the birth line (the dotted line on Fig. 2). The initial value of the magnetic field, which determines the spin period derivative, is drawn from a flat distribution as described in Section 2.3.

The binary starts on the zero age main sequence at $t = 0$. After 28.08 Myrs the first pulsar is born. At that time, the system consists of a pulsar and a massive rejuvenated companion. The neutron star initially evolves in the $P - \dot{P}$ plane along the line of constant magnetic field before turning down when the field decay becomes significant. At $t = 31.26$ Myrs the nuclear evolution of the companion plunges the system into the common envelope phase. The magnetic field of the pulsar is quenched and it falls close to the death line without changing the spin period. The companion loses its envelope and becomes a helium star while the neutron star reappears in the radio. Its \dot{P} is very small now so that it barely evolves until the second mass transfer occurs. This mass transfer is a stable Roche lobe overflow and commences at $t = 31.39$ Myrs. The system becomes an

X-ray binary and the neutron star is mildly recycled to a period ≈ 0.01 s. The amount of accreted matter is very small ($\sim 10^{-5} M_{\odot}$), but in this model full recycling is allowed regardless of the total accreted mass. In many other models (the ones without F in their name) we limit the accretion rate to the Eddington limit and consequently the recycling is weaker. Soon after this mass transfer, at $t = 37.11$ Myrs, the second pulsar is born, and for the following 23 Myrs the binary contains two radio loud pulsars. The second pulsar will evolve similarly to the first one. Initially it moves along the constant field line. As a consequence of our short field decay timescale it turns down and moves almost vertically. No mass transfers can occur as both stars are past the supernova explosion. At around $t = 50.74$ Myrs the second born pulsar falls below the death line. At this stage the system contains a mildly recycled pulsar which slowly evolves to the death line. It does not reach it throughout the whole simulation, which ends after 10 Gyrs. Some of the pulsars in our simulations manage to pass the death line before coalescence. This binary is relatively wide, so it does not coalesce within that time.

3.2 Population on the $P - \dot{P}$ diagram

In order to analyse the properties of the population of DNS we have to take the selection effects into account. We define two types of selection effects that lead to differences between the intrinsic and observed population. The first effect is related to the sensitivity of the telescope, the properties of the pulsar and the ISM along the line of sight. We have modelled these selection effects to reflect those that affected Parkes Multibeam Pulsar Survey, as described in Section 2.4. Additionally, it has been noted that binaries with an orbital period between 0.3 and 4h are difficult to detect (Faulkner 2004). Therefore we remove these systems from the observed population. The latter effect proves to be insignificant when it comes to the statistical properties of the observed pulsars, except for their binary periods.

We start with the analysis of the population of DNS systems on the $P - \dot{P}$ diagram. To obtain the present observable population of binary neutron stars we assume that the star formation rate in the galaxy is constant. We position the binaries in the Galaxy according to the model described in Section 2.3.11. Then we propagate them in the Galactic potential, giving them the additional kick velocities that they receive from the supernova explosions. We then look for the observable population taking into account the described selection effects. The density of the objects in the $P - \dot{P}$ plane is the total time that each pulsar spends in a given cell on the $\log P - \log \dot{P}$ plane, i.e. the density in a given cell is :

$$f_{ij} = \frac{F_{ij}}{F} \frac{1}{\Delta \log P \Delta \log \dot{P}}, \quad (28)$$

where $\Delta \log(P/1s) = 0.091$ and $\Delta \log(\dot{P}/1s^{-1}) = 0.261$ denote the bin width of the spin period and its derivative respectively, $F = \sum_{i,j=1}^{44} F_{ij}$ and

$$F_{ij} = \sum_{p=1}^{N_{ij}} t_{ij}^p f_{beaming}^p, \quad (29)$$

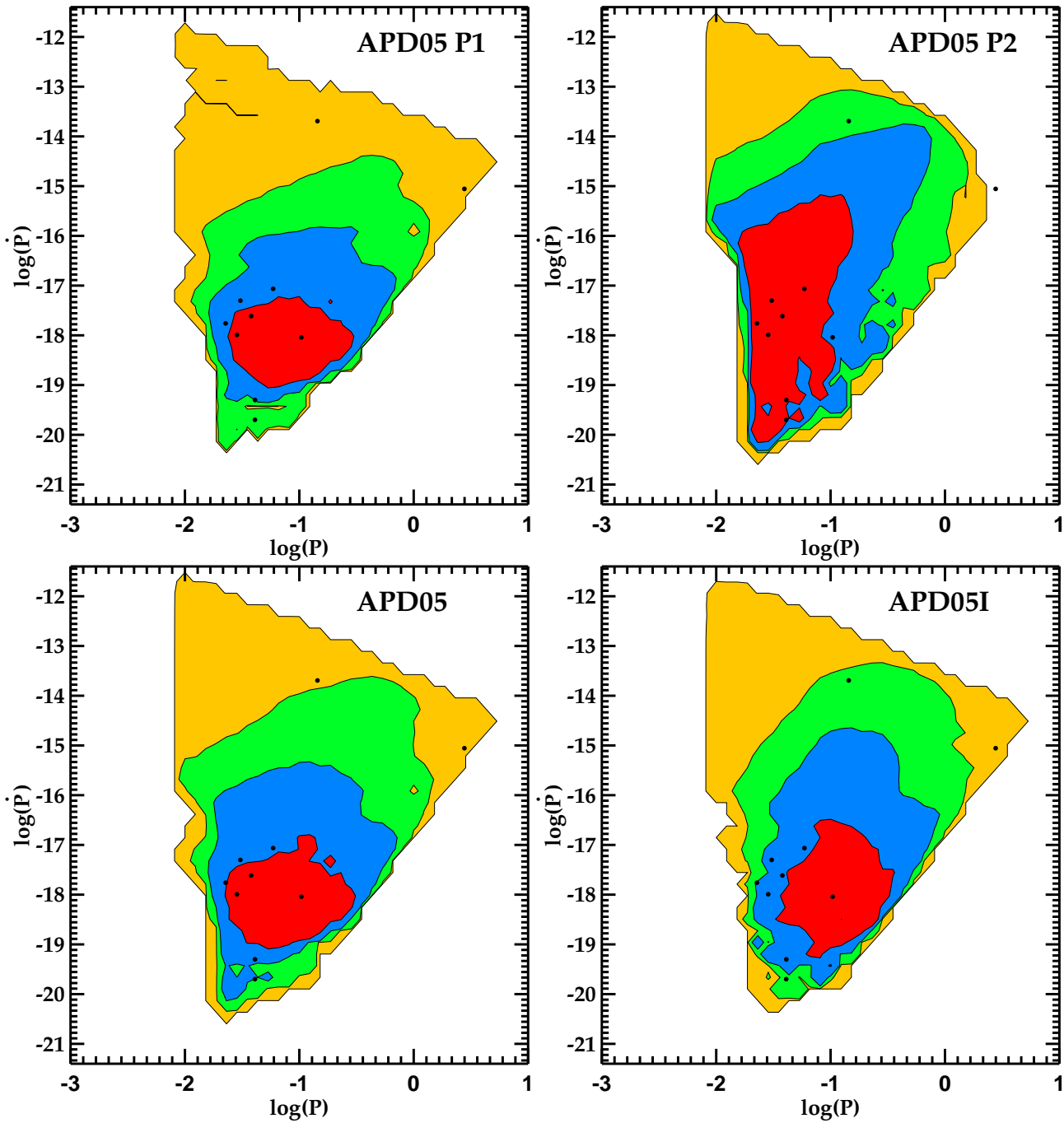


Figure 3. Probability density on $P - \dot{P}$ diagram for APD05 model, for both first and second born pulsars separately (P1 and P2, respectively), for both pulsars together and for the APD05I model, where a flat distribution of initial spin periods is assumed. The levels correspond to contours containing 68, 95 and 99 percent of the objects. Black points correspond to observations.

where N_{ij} is the number of simulated pulsars with P contained in the i -th and \dot{P} in j -th bin and t_{ij}^p is the time the p -th pulsar spends in these bins and $f_{beaming}^p$ is the beaming factor for p -th pulsar at a given time. The range of $\log_{10} P$ from -3 to 1 as well as the $\log_{10} \dot{P}$ range from -21.5 to -11 were divided into 44 bins.

The density of the population in the $P - \dot{P}$ plane (shown on Fig. 3 and its continuations) is strongly affected by the radio selection effects. The properties of first and second born pulsars contribute to this density. In majority of the

models, the first born pulsar will dominate, as it is mildly recycled and emits longer in the radio. The details of the binary evolution and the recycling process strongly influence the region where we expect the recycled pulsars to be.

All the binary systems in each model have been assigned four sets of initial parameters, the values of which were randomly chosen, in order to check how much the results can vary. The presented $P - \dot{P}$ diagrams are an average of these four simulation runs. Removing a small number of systems

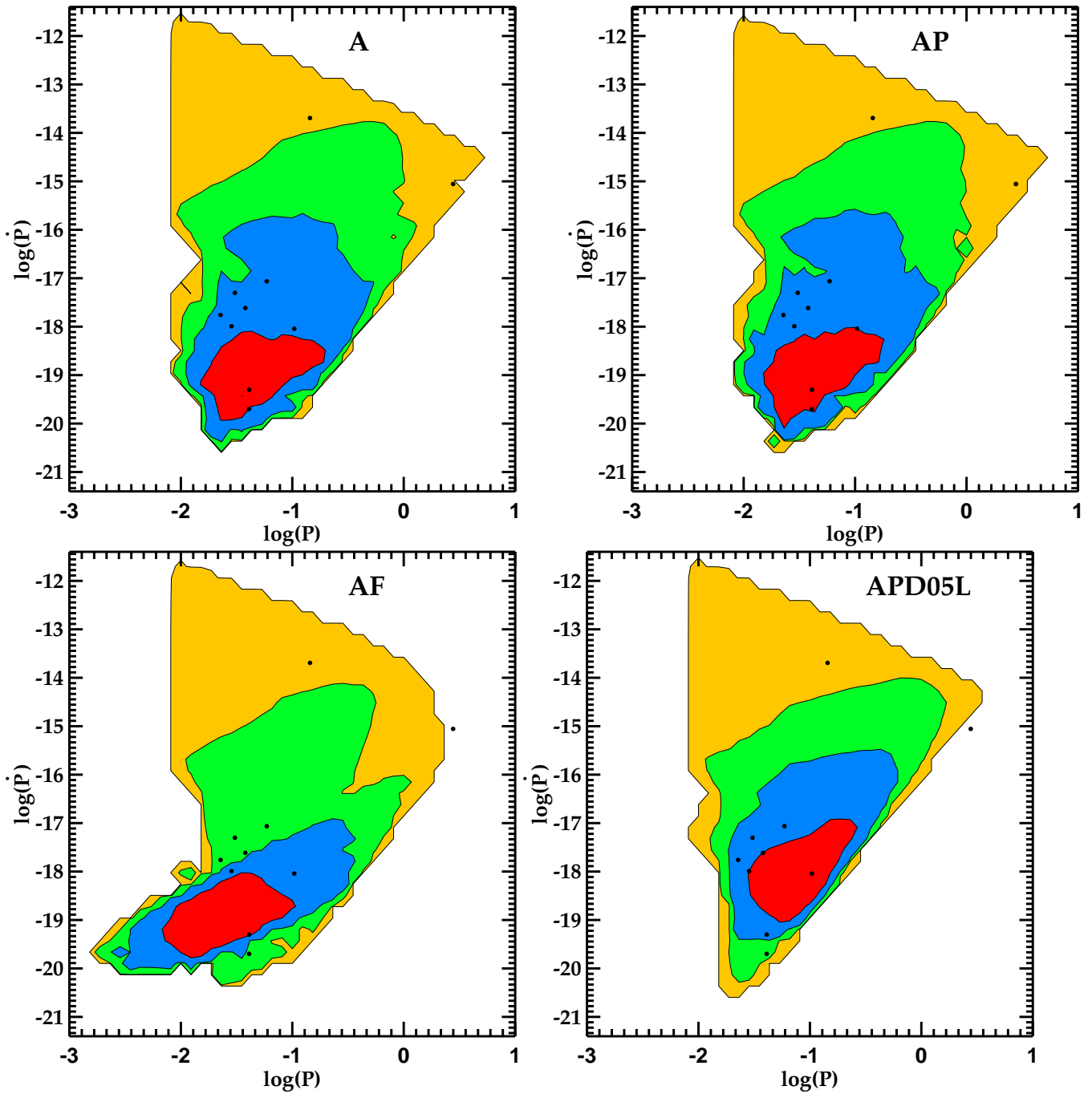


Figure 3 – *continued* Probability density on $P - \dot{P}$ diagram for the A, AP, AF and APD05L models. The levels correspond to contours containing 68, 95 and 99 percent of the objects. The outer contour delimits the region containing all the objects in the simulation. Black points correspond to observations.

and adding another realization of any given model did not affect the results significantly.

The first two plots show the probability densities on the $P - \dot{P}$ diagram for the first and second pulsar in our best model, APD05 (APD05 P1 and APD05 P2 respectively). In this model we consider the inefficient propeller effect and increase the mass scale of accretion induced field decay to $0.05M_{\odot}$. It is clear that the first born pulsars are concentrated in the region of mildly recycled pulsars. The pulsars which are born second evolve very simply. Initially they fol-

low the lines of constant magnetic field and after few million years they quickly move down. This is because of the short field decay timescale. The combined population is shown on the plot denoted by APD05. It resembles the plot showing the first born pulsar. This is expected, as the mildly recycled pulsars evolve along the constant magnetic field line. Hence they spend a long time in the most densely populated region. The total contribution of the second born pulsar to this model is only 15%. The only problem with this model

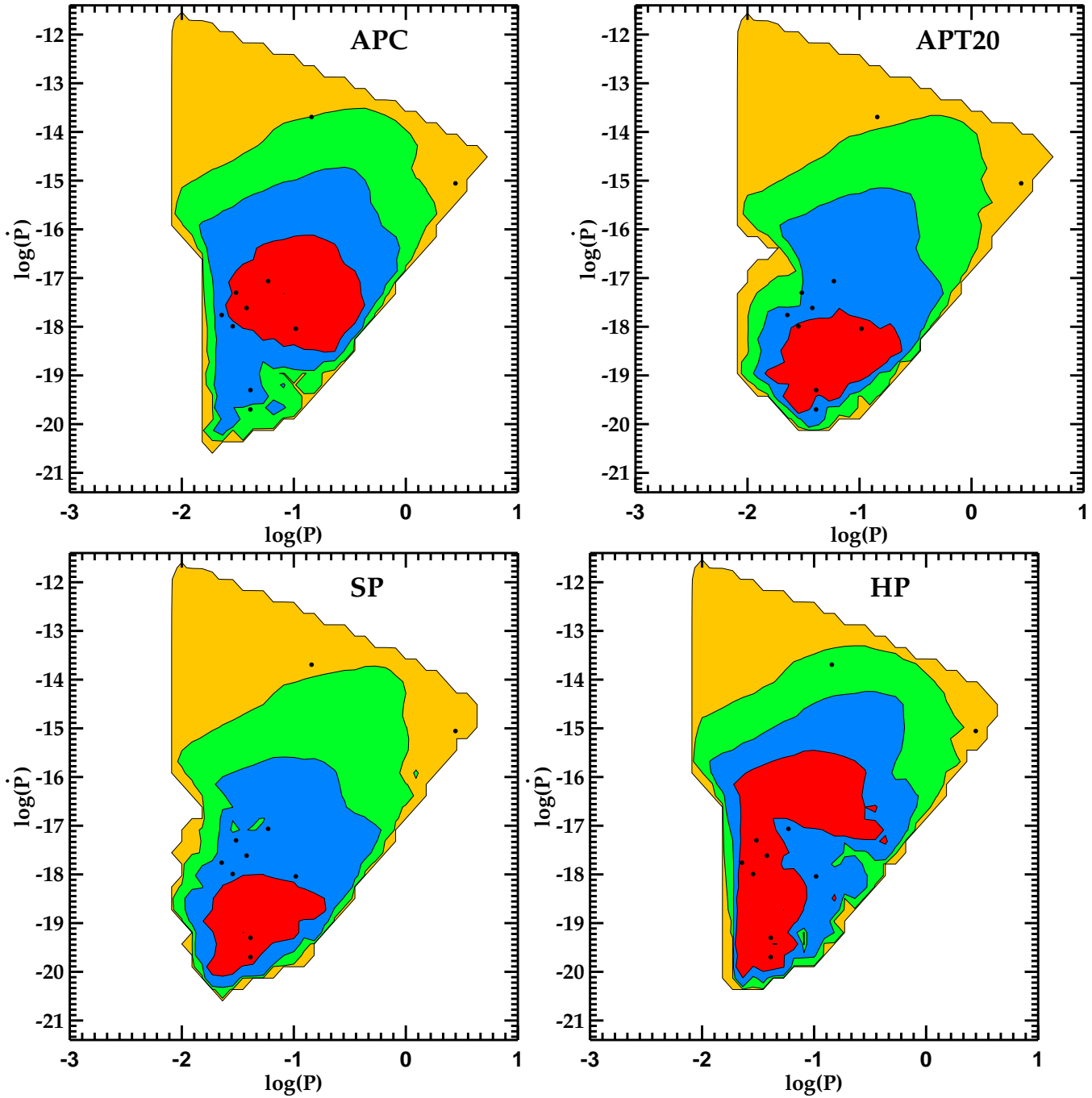


Figure 3 – *continued* Probability density on $P - \dot{P}$ diagram for the APC, APT20, SP and HP models. The levels correspond to contours containing 68, 95 and 99 percent of the objects. Black points correspond to observations.

is that J1518+4904 and J1829+2456 are at the edge of the low density regions.

The next plot, showing the APD05I model, is again quite similar. The difference here is that the initial spin periods are chosen randomly in a range from 10 to 100 ms. Introducing the slower spinning pulsars shifts the whole population towards longer periods. Note that many of the observed pulsars now fall in the lower density regions. This results in a smaller likelihood of this model (see Section 3.4). For the other models, we keep the assumption of a constant $P_{ini} = 10$ ms for each pulsar. Without this assumption it is

harder to recycle our pulsars enough to match the observed population, unless the accretion physics is altered.

The next four plots present the A, AP, AF and APD05L models. The first one is the model based on our initial estimates of the evolutionary parameters. It predicts too many pulsars with very small \dot{P} (of the order of 10^{-19}). Replacing the propeller effect with our modified prescription improves the situation only slightly, as demonstrated by the AP model. The highest probability density extends now to somewhat higher, but still too low, \dot{P} values. The relatively small number of binaries in which the propeller effect takes

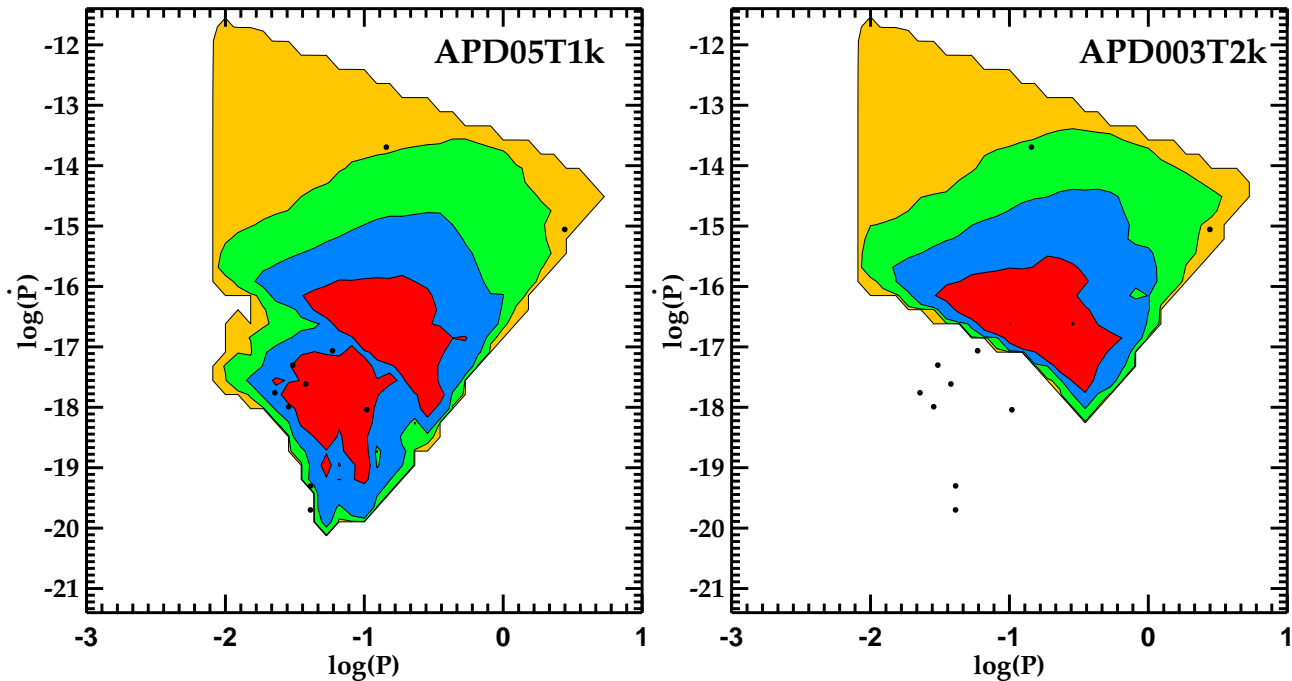


Figure 3 – *continued* Probability density on $P-\dot{P}$ diagram for the APD05T1k and APD003T2k models. The levels correspond to contours containing 68, 95 and 99 percent of the objects. The outer contour delimits the region containing all the objects in the simulation. Black points correspond to observations.

place, explains why this change has such a small impact. Next, we present a model with full recycling regardless of the amount of matter accreted - the AF model. In this case, the population of the recycled pulsars extends to periods below 20 ms. There are no such pulsars observed in the DNS systems.

As mentioned in the Section 2.3.8, we present the APD05L model. This is a variation of the APD05 model with the radio luminosity law defined by Equation 16. This model looks more like the AP or A model with the contour containing 68% of the systems moved to slower rotators with higher \dot{P} values, rather than like the APD05 model it originates from. Based on this model’s low likelihood, we decide that the luminosity prescription of Narayan & Ostriker (1990) yields better results in our models.

We then consider what happens when we do not allow any accretion during the CE phase. The corresponding model, APC, is similar to the APD05 model, but it is more likely now to find pulsars with higher values of \dot{P} . This directly follows from lack of accretion in the CE phase. Without the accretion, each pulsar will have a stronger magnetic field on average. This effect would be even more pronounced, but the first born pulsars will have more time to quench their magnetic field, as we allow them to do that until the first accretion takes place.

Next we check how the timescale of the spontaneous decay of magnetic field influences the overall shape of the distribution in the $P-\dot{P}$ diagram, see the AP and APT20 model. Changing the timescale to 20 Myrs does not have a big effect. The highest density region is concentrated around higher \dot{P} as the magnetic field is stronger for the majority of pulsars. Another change is that the pulsars will start moving

down vertically when they reach longer spin periods. This is a direct consequence of the longer decay timescale.

Before considering even longer timescales, we first turn to the two models based on the different STARTRACK stellar evolution models, namely the SP and HP models. The SP model only differs from the AP in the way the initial masses are calculated. As expected, the SP and AP look very much alike. The contribution of the second born pulsar to the total density in the $P-\dot{P}$ space in this model is $\sim 12\%$. Differences will be visible in the distribution of the chirp masses and the density in the primary mass versus the mass ratio planes, see Section 4. The HP model includes the hyper-critical accretion in the CE phase, which leads to many pulsars having the weakest allowed magnetic field. These pulsars fall below the death line and are no longer emitting in the radio. During the next accretion event they could in principle be recycled and become millisecond pulsars, but in the binaries that give rise to double neutron star this second accretion phase will be too short and will not spin them up enough. The vertical part of the high density contour originates mainly from the second born pulsars (compare with APD05 P2). The part that roughly follows the constant field lines comes from the first born pulsars that have only experienced a stable mass transfer. After the accretion phase they move along the constant field lines. As much as 68% of the contribution to the total density in the $P-\dot{P}$ space comes from the second born pulsar, as opposed to $\sim 15\%$ for models based on the A STARTRACK mode or $\sim 12\%$ for the SP model.

Finally, we come back to the question of the timescale of the magnetic field decay. We present two different models. At first, we show the ADP05T1k model, which is the same as the APD05, but with $\tau_d = 1000\text{Myr}$ and a field

decay occurring throughout the lifetime of a pulsar. The contour containing 68 % of the total density is split into two separate regions. One of them, at high \dot{P} values, is populated by the second born pulsars and the first born pulsars that did not accrete any matter. The second, with the lower values of \dot{P} , is filled by the pulsars that have been spun up. This model clearly struggles to explain the existence of the two observed pulsars with a small \dot{P} , J1518+4904 and J1829+2456. The second model, APD003T2k, adopts the values of $\tau_d = 2000\text{Myrs}$ and $\Delta M_d = 0.0033$ from the best model of Kiel et al. (2008). Note that we do not correlate the initial spin periods with the magnetic fields. The lowered ΔM_d results in all the pulsars accreting during the CE phase being removed from the visible population. The top part of the $P - \dot{P}$ diagram corresponds to the pulsars evolving without any interactions and is very similar to the corresponding region of the APD05T1k model. The next model we test is the APD003T2kC model. It is based on the APD003T2k, but without any accretion in the CE phase allowed. We do not show a plot for this model as it looks virtually the same as the one for APD003T2k. This may seem surprising since we argue that the CE phase is the main process shaping the distribution of pulsars in the $P - \dot{P}$ space for that model. During RLOF only a small amount of matter is accreted, of the order of $10^{-5} M_\odot$. This is not enough to significantly affect the neutron star with a still strong magnetic field. After the accretion the star will simply continue its evolution with very similar values of P and \dot{P} , almost as if no accretion occurred. Therefore the accreting and the second born pulsar will evolve essentially likewise. In this model, there would be more pulsars visible in radio than in the APD003T2k model, but the probability density on the $P - \dot{P}$ is similar in both cases. The same reasoning applies to the APD05T1kC model (that is APD05T1k without any accretion in the CE phase) - it will look very similar to APD003T1k.

3.3 Radio-detected fraction

Currently the known sample of double neutron stars is very scarce. Future instruments like SKA should change this. In Fig. 4 we present the fraction of observed radio pulsars as a function of the signal-to-noise ratio limit for the detection with the Parkes Multibeam Pulsar Survey (PMBPS). With the realistic limit of 10 sigma, we only see $\approx 5\%$ of the simulated population. To detect the majority of population we would need to increase the sensitivity of detectors by at least a factor of 10. With a larger observed sample we could check the models much more precisely by repeating the same analysis as in this work. With the currently available limited sample we are having problems constraining the evolutionary parameters. Note that we have used the parameters of the PMBPS for the selection effects but we simulate observations of the whole sky. The main for this reason is that choosing a region of sky that was observed by the PMBPS would significantly reduce our statistics. Since we neither distinguish between the regions of galaxy when injecting the simulated pulsars nor correlate the initial spin and/or the magnetic field with supernova properties, the population observed in any part of the sky should have equivalent statistical properties as the total population. We checked that by simulating observations of a smaller patch of sky, corre-

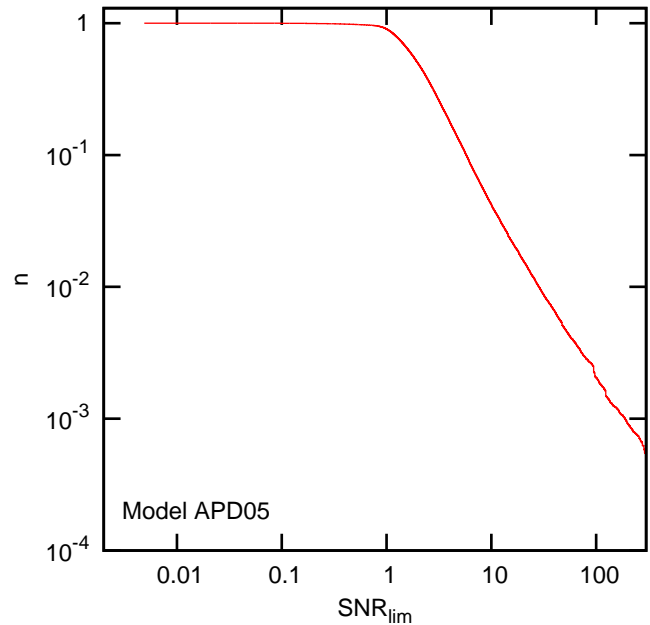


Figure 4. Cumulative fraction of pulsars detected as a function of limiting signal-to-noise ratio for the Parkes Multibeam Pulsar Survey.

sponding to the PMBPS, and the results were virtually the same.

3.4 Comparison with observations

In order to quantify which model of the distribution in the $P - \dot{P}$ best describes the data we calculate the likelihood of each model given the data from Table 1. We define the likelihood as :

$$\mathcal{L} = \prod_k^K f(P_k, \dot{P}_k), \quad (30)$$

where P_k and \dot{P}_k are the spin period and its derivative values for the k -th real observed pulsar (see Table 1) and f is the probability density defined by Equation 28 in Section 3.2. We use two sets of data to calculate the likelihood: the first set excludes both J0737-3039 A and B as their orbital period is in the range prohibited by one of our selection effects (see Section 1.2). Another special case we exclude is the B2127+11C pulsar as it probably had a different dynamical history and does not provide good constraints on the models; the second set does not contain J0737-3039 B, which is no longer visible, and B2127+11C for the same reason as above. The latter comparison includes J0737-3039 A as we argue that the selection effect based on the orbital period is not significant.

Likelihood values are presented in Table 4. In both comparisons with observations, the model HP and APD05 are the two best models. The HP model predicts a very unusual shape of the $P - \dot{P}$ distribution, even though it has a high likelihood. Another argument against this model is the distribution of chirp masses, see Section 4. Therefore we will focus on the APD05 as our best model. This is a model with the inefficient propeller effect taken into account and with increased mass scale for the magnetic field decay. The

Table 4. The logarithm of the likelihood for all models. Comparison with observations: case 1) excluding J0737-3039 A and B and B2127+11C; case 2) excluding J0737-3039 B and B2127+11C. The $-\ln$ values originate in J1518+4904 (APD05T1k) and most pulsars (APD003T2k) lying in the regions were the modelled probability density is null.

Comparison	1	2
A	-9.82	-11.68
AF	-12.67	-16.23
AP	-9.72	-11.56
APC	-10.63	-13.37
APD05	-9.59	-11.08
APD05I	-11.13	-13.49
APD05T1k	-inf	-inf
APD003T2k	-inf	-inf
APD05L	-11.26	-13.12
APT20	-10.44	-12.02
HP	-8.69	-10.87
SP	-9.74	-11.57

models with the standard value lead to too weak magnetic field of the synthetic sample. Increasing the magnetic field mass decay scale ΔM_d leads to a smaller decay of the field during accretion and therefore a better agreement with the data. The models with full recycling are very far from the observations since they predict the population of pulsars in binaries with spin periods below 20ms. The models with very long timescales of the field decay have formally $-\ln$ likelihood as some of the pulsars fall into bins with no simulated pulsars. We have verified that the results are not very sensitive to the number and size of the bins chosen in for the $P - \dot{P}$ diagram by repeating the likelihood analysis with different values of this parameters.

We think that this method provides a reasonable quantitative comparison between models and observations. In our case it is somewhat limited by the small sample of observed DNSs. For other synthetic population it could prove more useful.

4 EXPECTED MASSES OF NEUTRON STARS OBSERVED IN GRAVITATIONAL WAVES AND IN THE RADIO

In Bulik et al. (2004) the authors have calculated the expected masses of neutron stars observed in gravitational waves using the STARTRACK population synthesis code. The assumed value of the minimum mass and maximum mass of a neutron star was $1.2 M_\odot$ and $3.0 M_\odot$ respectively. They have verified the results by taking the maximum mass to be $2 M_\odot$ and $2.5 M_\odot$ (Gondek-Rosińska et al. 2005a). The distributions of the mass ratio q (defined as the ratio of less to more massive component) of neutron star binaries observed in gravitational waves were shown to have two peaks: the first one for nearly equal mass systems with both masses close to $1.4 M_\odot$; and the second one with a small mass ratio $q \sim 0.6 - 0.7$ in binaries consisting of a neutron star with gravitational mass close to the maximum mass with a relatively smaller companion. The strength of the second peak depends on the value of the maximum mass of a neutron star. For the models with the higher maximal mass

the sample starts to be dominated by binaries belonging to the second peak. The authors used 20 additional models of stellar evolution, where they have varied the parameters describing various stages of stellar and binary evolution in order to assess the robustness of the results. In that paper, the gravitational wave selected sample was compared with the volume limited sample. The volume limited sample contained only the binaries potentially detectable in gravitational waves, i.e. those younger than 10Gyr.

Up to now there was no detailed comparison of properties of neutron star binaries observed in the radio and gravitational waves. The only paper (Gondek-Rosińska et al. 2005b) that dealt with a similar problem contained a discussion of radio observability of the gravitational wave selected sample, within a single model of binary evolution with a wide initial neutron star mass spectrum. The authors assumed that the radio selected sample only consists of binaries with lifetimes (from formation till merger) longer than 100 Myrs. There was no upper limit on the radio lifetime other than the Hubble time. The neutron stars in this sample were observable as pulsars for the entire lifetime of the binary. In that paper it was shown that binary radio pulsars, which all had long orbital periods, were only a few percent of all binary neutron stars observed in gravitational waves. The DNSs observed in the radio had a mass ratio distribution clustered around unity. The long lived systems evolved without the possibility of significant accretion onto a neutron star, while the short lived systems (with $t_{\text{grav}} < 100$ Myrs) did undergo common envelope episodes with hypercritical accretion onto the neutron star. These common envelope episodes had two consequences: they tightened the orbits and led to a decrease of the mass ratio of the final double neutron star system, as one of the neutron stars accreted some matter. This implied that the mass distribution of the gravitational wave selected sample of double neutron star binaries was different than the radio selected one.

Here we present a comparison of the radio selected sample of double neutron star binaries with the observed sample, taking into account the selection effects. In this way we choose the best model and compare the corresponding radio population with the one selected in gravitational waves. The radio population also contains the binaries with merger times greater than the Hubble time that were omitted in previous efforts.

In Fig. 5 we present the simulated distributions of objects in the plane spanned by the mass ratio and the primary mass, defined as the mass of the more massive component of a binary, for APD05, HP and SP models. The left panels correspond to the radio selected sample, while the right panels show the gravitational wave selected ones. The objects contained in the radio sample are weighted by the time they are observable as a pulsar from Earth, while the objects in the gravitational wave selected sample are weighted by the volume in which they are detectable (see 2.5). The solid lines correspond to constant values of the chirp mass in these coordinates. The observed DNS systems are shown as black points. Note that the masses of neutron stars in the binaries lying in the middle of the plots (corresponding to J1811-1736 and J1518+4904) are poorly constrained.

In addition, in Fig. 6 we compare the chirp mass distributions of the binaries selected by their observability in the radio band and in the gravitational waves. Comparing

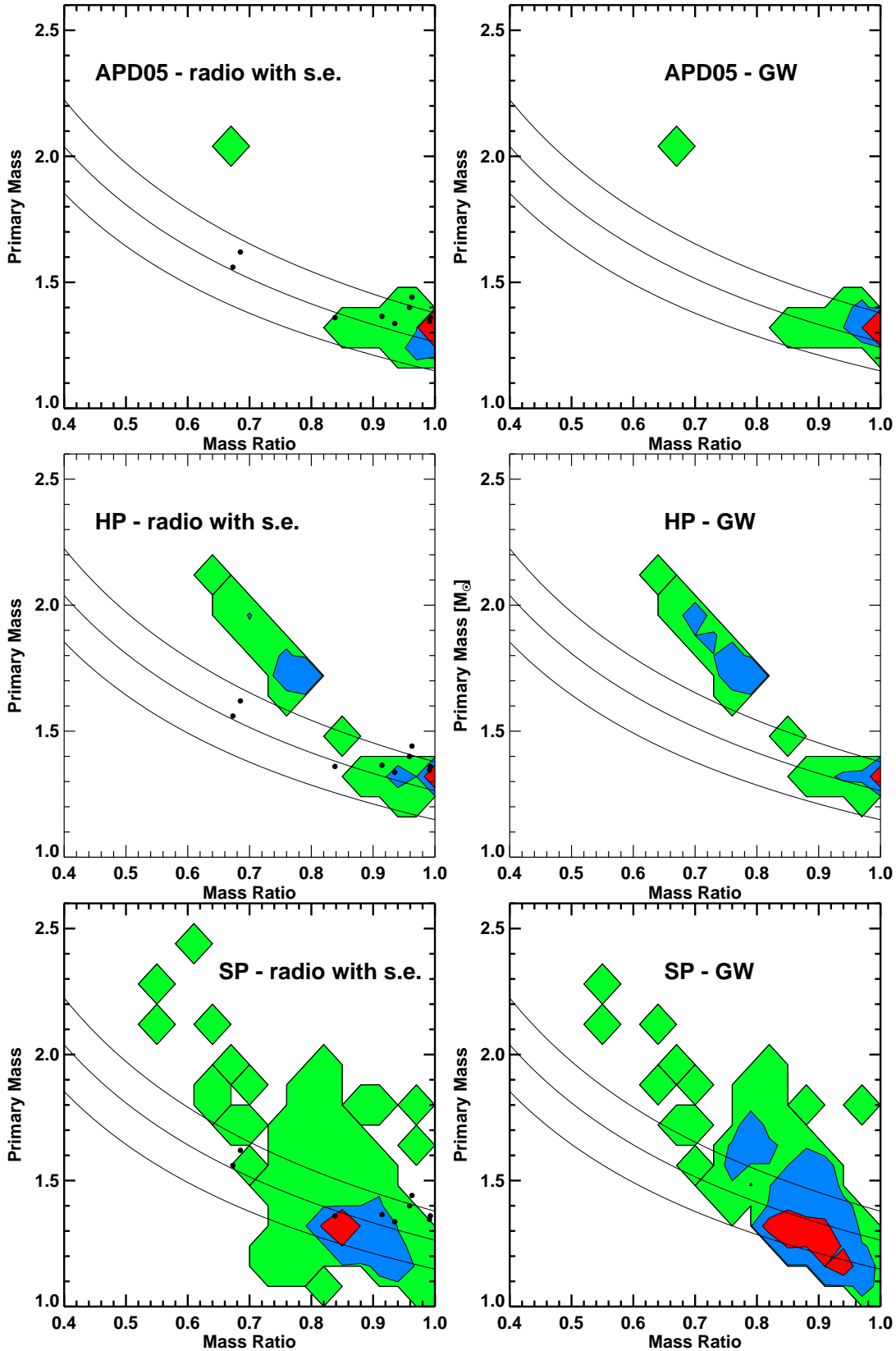


Figure 5. Normalised distribution of masses and mass ratios for the simulated populations observable in the radio (left panels) and gravitational waves (right panels). The shadings represents the regions containing 68%, 95% , and all the systems. In each panel we show the lines corresponding to constant chirp masses of 1.0, 1.1, 1.2 M_{\odot} . Black points correspond to observations.

our radio selected sample with the data from Table 1, we see that the APD05 (top panel) and SP (lower panel) models are more consistent with the observations than the HP (middle panel) model in which the majority of binary radio pulsars are predicted to have $q < 0.8$ and one massive neutron star with $m_2 > 1.6M_\odot$. The APD05 model, which reproduces best the observed distribution of pulsars in the $P - \dot{P}$ space, is consistent with most of the observed binary radio pulsars. It reproduces the chirp mass distribution of the radio observed sample well. The low chirp mass systems are not very likely in this model, but possible. The binary neutron stars with low mass ratios and moderate masses are not predicted in this model. However, one must take into account the fact that the mass measurements of J1811-1736 and J1518+4904 have quite large error bars. The SP model is close to reproducing the distribution of the masses and mass ratios of all observed neutron star binaries. In this model the distribution of masses is wide. It predicts the existence of binaries containing massive neutron stars, however the radio selected distribution is concentrated around $q \sim 0.8 - 0.9$ and primary masses $\sim 1.35M_\odot$.

A comparison of the radio selected sample with the gravitational wave one shows visible differences for SP and HP models and negligible ones for the APD05 model (see also Fig. 6). In the APD05 model, the two samples are very similar, as expected. This is due to the fact that in the standard STARTRACK model (see Section 2.2.1) the range of masses of newborn neutron stars is narrow compared to the previous calculations. In addition, the amount of matter accreted during the common envelope phase with a helium star is negligible.

In the HP model both the radio and gravitational wave sample has a large fraction of unequal mass binaries with $q = 0.7$ and $m_2 \approx 1.7M_\odot$. However, the main peak in the distribution of the chirp mass is for binaries with both components of about $1.4M_\odot$. This model fails to reproduce the radio observed distribution of masses and mass ratios. At the same time, this model is the only one able to explain the existence of binaries with a high chirp mass ($M_{chirp} > 1.3M_\odot$), if such binaries exist. It is possible to form these high mass binaries because of the hypercritical accretion rate.

In the SP model the gravitational wave selected sample has a tail towards the higher chirp mass values which is more pronounced with respect to the radio selected one. This is because of the volume effect: the sampling volume scales as $\propto M_{chirp}^{5/2}$. Thus, the heavier binaries are observable in a much larger volume in gravitational waves. The mass ratio distribution of the gravitational wave selected sample leans towards lower values because the unequal mass binaries typically contain a low mass neutron star with a more massive companion. They have a higher chirp mass than the equal mass neutron star binaries, that typically contain two stars with low masses. This is similar to the comparison between the gravitational wave selected and the volume limited sample presented in Bulik et al. (2004). The comparison with radio observations reveals quite an interesting feature: the distribution of chirp masses is underestimated in this model. However, the observed mass ratios are relatively well reproduced, as this model leads to a wide distribution of radio observed mass ratios.

In the APD05 model, the initial masses of the neutron stars come from a very narrow range. We do not allow a

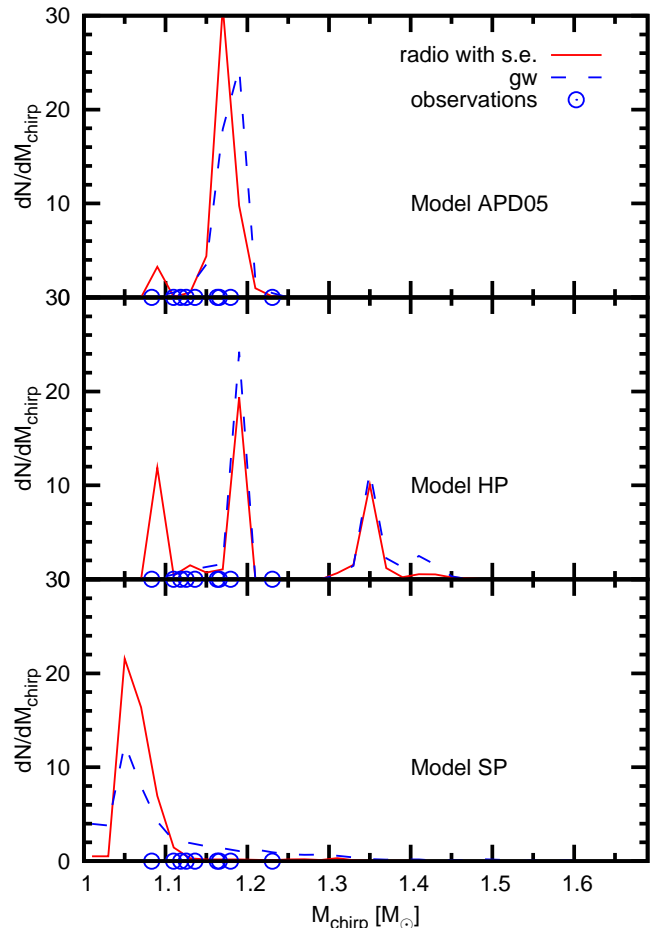


Figure 6. The normalised distributions of chirp masses for the simulated gravitational waves (solid) and radio (dashed) selected samples of double neutron star binaries. Top panel shows model APD05, middle panel HP and SP is shown in the bottom panel. Circles on the axes lie where the observed binaries are. The observed sample is too small to build a distribution.

substantial accretion. Thus most neutron star binaries have similar masses and there is no possibility to form binaries with different chirp masses or mass ratios in this model. Hence, there are small differences between their distributions for the gravitational wave and radio selected populations. This model reproduced the observed chirp masses reasonably well. The gravitational wave population is shifted towards higher chirp masses due to the volume effect, as described above for the SP model.

5 CONCLUSIONS

We have modeled the evolution of binary stars leading to the formation of double neutron star systems. We then follow their evolution as pulsars and discuss the properties of the double neutron stars observable in the radio. We discuss several models and compare the expected distribution with observations in the $P - \dot{P}$ space using likelihood methods that can easily be applied to other synthesis studies. In our case, where the observed sample consists of mildly recycled pulsars, the likelihood method favours different models

than when modelling single pulsars. The second born pulsar evolves identically to solitary ones, however their contribution to the overall density on the $P-\dot{P}$ diagram is small.

First of all, the analysis of the binary star evolution provides little constraints on the spontaneous magnetic field decay. This was to be expected as DNSs are typically observed to be old and evolved objects. At the same time, we see that there must be some mechanism at work which leads to a decay of the magnetic field of the first born star. This can either be the spontaneous magnetic field decay, mentioned above, or the magnetic field decay due to accretion. However, we noticed that in the best fitting models the amount of accreted matter is small. This is due to the time for the accretion being short, which is a consequence of the fast evolutionary timescale of the companion. Moreover, the model with large mass decay scale fits the data better than the one with a small value. Thus, in double neutron stars the spontaneous field decay seems to be much more important than the accretion induced decay. However, in our model we have assumed that the decay timescale is very short (few Myr), which does not necessarily provide a good model for the evolution of isolated pulsars. We argue that the fact that one can get a good fit to the observations of mildly recycled pulsars in DNS systems suggests that this quick quenching mimics spin evolution of young pulsars well. Another option present in the literature is to correlate the initial spin periods with the magnetic field strength.

The models in which we allow for substantial accretion and recycling of the neutron star lead to formation of a large number of binaries with periods below 20 ms and period derivatives below 10^{-18} ss^{-1} . There are no observed DNSs with such short periods, which means that such substantial accretion does not take place. Thus the mass accreted by the first born star must be small, and the efficiency of recycling during common envelope is very low. This efficiency can be much smaller than in the case of a stable mass transfer. We do not expect a steady transfer of angular momentum as the mass transfer can be turbulent.

If the angular momentum transferred is low, then we do not expect double neutron stars to have pulsation periods below ≈ 20 ms. The binaries containing pulsars with a shorter period are probably neutron star - white dwarf binaries, in which the mass transfer had been stable and lasted much longer than in the progenitors of the double neutron star systems.

Other studies of synthetic pulsar populations have not made comparisons between the pulsars detectable by their emission in the radio and these emitting gravitational waves. We also find that the model resembling the best one from Kiel et al. (2008) does not produce good results in our case. Double neutron star systems contain pulsars which are recycled, but only mildly and would not be called classical recycled pulsars. It is difficult to produce this kind of systems in the model based on work by Kiel et al. (2008). The main problem arises from the fact that the pulsar's magnetic field needs to be quenched without a significant spin-up. Possibly our understanding of the accretion physics is incomplete and future studies could solve the problem with spinning up those mildly recycled pulsars.

We compare the properties of the radio selected and gravitational wave selected sample. We find that the APD05 model is most consistent with observations. It not only

matches the observed sample in the $P - \dot{P}$ space, but it also reproduces the distribution of chirp masses reasonably well. In this model, the binary evolution proceeds within the standard STARTRACK model, we allow for the inefficient propeller effect, partial spin-up proportional to the amount of mass accreted takes place, and mass scale of magnetic field decay is increased to $M_d = 0.05 M_\odot$. There are hardly any differences between the distribution of masses in the radio and gravitational wave selected samples. The mass ratio of double neutron stars is close to unity in both the radio and gravitational wave selected sample. However, radio observations show that there are systems with a mass ratio likely to be in the range of 0.6 – 0.9, which do not appear in this model. The presence of such objects can be explained by assuming the initial mass spectrum of neutron stars is wide, like the one in the SP model. The presence of such binaries suggests that the unequal mass systems with a mass ratio in the range of 0.7 to unity should be included in the search for gravitational wave signals. Including a wider initial mass range on one hand widens the expected distribution of mass ratios, but on the other hand decreases the agreement between the expected and observed distribution of chirp masses in the radio. The HP model predicts existence of very high chirp mass systems, none of which has been discovered. As this model is dominated by the second born pulsars, this suggests that the observed pulsars are the first born, mildly recycled objects.

The models based on the STARTRACK standard model have similar predictions for the differences between the populations detectable in the radio and gravitational waves, regardless of the subsequent pulsar evolution details. Future work should include a bigger observational sample and a wider range of object types. This should allow to better constrain the pulsar evolution models.

This conclusions may be verified with Square Kilometer Array observations that should reveal many more DNS systems. The measurement of their masses along with the identification of the DNS merging population by the Advanced LIGO and VIRGO will provide further insight into the properties of the population of double neutron stars.

ACKNOWLEDGMENTS

This research was supported in part by the Polish Ministry of National Education (MENiSW) under grants No. N 202 2318 37, 1PO3D00530, N203 302835, N N203 511 238, DPN/N176/VIRGO/200, by the European Gravitational Observatory grant EGO-DIR-102-2007, by the FO-CUS Programme of Foundation for Polish Science and by CompStar, a Research Networking Programme of the European Science Foundation. Authors would also like to thank Matthew Bailes for help with improving our treatment of radio selection effects, sharing the PSREVOLVE code and for his patience. Discussions about pulsar masses with Ingrid Stairs have been very fruitful as well. The anonymous referee's comments helped to improve our work and we found them very useful. We are grateful to Evelyn Caris alias Reynders and Willem van Straten for their help with the manuscript.

REFERENCES

- Abramovici A., Althouse W. E., Drever R. W. P., Gursel Y., Kawamura S., Raab F. J., Shoemaker D., Sievers L., Spero R. E., Thorne K. S., 1992, *Science*, 256, 325
- Arzoumanian Z., Chernoff D. F., Cordes J. M., 2002, *ApJ*, 568, 289
- Arzoumanian Z., Cordes J. M., Wasserman I., 1999, *ApJ*, 520, 696
- Belczynski K., Bulik T., 2002, *ApJ Lett*, 574, L147
- Belczynski K., Bulik T., Kluźniak W. I., 2002, *ApJ Lett*, 567, L63
- Belczynski K., Bulik T., Rudak B., 2002, *ApJ*, 571, 394
- Belczynski K., Kalogera V., 2001, *ApJ Lett*, 550, L183
- Belczynski K., Kalogera V., Bulik T., 2002, *ApJ*, 572, 407
- Belczynski K., Kalogera V., Rasio F. A., Taam R. E., Zezas A., Bulik T., Maccarone T. J., Ivanova N., 2008, *ApJS*, 174, 223
- Benensohn J. S., Lamb D. Q., Taam R. E., 1997, *ApJ*, 478, 723
- Bethe H. A., Brown G. E., 1998, *ApJ*, 506, 780
- Bhat N. D. R., Cordes J. M., Camilo F., Nice D. J., Lorimer D. R., 2004, *ApJ*, 605, 759
- Bhattacharya D., Wijers R. A. M. J., Hartman J. W., Verbunt F., 1992, *A&A*, 254, 198
- Bisnovatyi-Kogan G. S., Komberg B. V., 1974, *Soviet Astron.*, 18, 217
- Blaes O., Rajagopal M., 1991, *ApJ*, 381, 210
- Bogomazov A. I., Abubekerov M. K., Lipunov V. M., Cherepashchuk A. M., 2005, *Astronomy Reports*, 49, 295
- Bondi H., Hoyle F., 1944, *MNRAS*, 104, 273
- Bradaschia C., Calloni E., Cobal M., Del Fabbro R., di Virgilio A., Giazotto A., Holloway L. E., Kautzky H., Michelozzi B., Montelatici V., Passuello D., Velloso W., 1991, in *Problems of Fundamental Modern Physics II VIRGO: a ground based interferometric antenna for gravitational wave detection above 10 Hz.* World Scientific, Singapore, pp 341–356
- Brandt N., Podsiadlowski P., 1995, *MNRAS*, 274, 461
- Brown G. E., Lee C.-H., Bethe H. A., 2000, *ApJ*, 541, 918
- Bulik T., Belczyński K., 2003, *ApJ Lett*, 589, L37
- Bulik T., Belczyński K., Rudak B., 2004, *A&A*, 415, 407
- Bulik T., Belczyński K., Zbijewski W., 1999, *MNRAS*, 309, 629
- Bulik T., Gondek-Rosinska D., Belczynski K., 2004, *MNRAS*, 352, 1372
- Buonanno A., Cook G. B., Pretorius F., 2007, *Phys. Rev. D*, 75, 124018
- Burgay M., D’Amico N., Possenti A., Manchester R. N., Lyne A. G., Joshi B. C., McLaughlin M. A., Kramer M., Sarkissian J. M., Camilo F., Kalogera V., Kim C., Lorimer D. R., 2003, *Nature*, 426, 531
- Burgay M., Joshi B. C., D’Amico N., Possenti A., Lyne A. G., Manchester R. N., McLaughlin M. A., Kramer M., Camilo F., Freire P. C. C., 2006, *MNRAS*, 368, 283
- Choudhuri A. R., Konar S., 2002, *MNRAS*, 332, 933
- Contopoulos I., Spitkovsky A., 2006, *ApJ*, 643, 1139
- Cordes J. M., Lazio T. J. W., 2002, *ArXiv Astrophysics e-prints*
- Cui W., 1997, *ApJ Lett*, 482, L163+
- Cumming A., Zweibel E., Bildsten L., 2001, *ApJ*, 557, 958
- D’Angelo C. R., Spruit H. C., 2010, *MNRAS*, 406, 1208
- de Kool M., 1990, *ApJ*, 358, 189
- Dewey R. J., Taylor J. H., Weisberg J. M., Stokes G. H., 1985, *ApJ Lett*, 294, L25
- Dewi J. D. M., Podsiadlowski P., Pols O. R., 2005, *MNRAS*, 363, L71
- Dewi J. D. M., Podsiadlowski P., Sena A., 2006, *MNRAS*, 368, 1742
- Emmering R. T., Chevalier R. A., 1989, *ApJ*, 345, 931
- Faucher-Giguère C.-A., Kaspi V. M., 2006, *ApJ*, 643, 332
- Faulkner A. J., 2004, PhD thesis, Faculty of Science and Engineering, University of Manchester
- Faulkner A. J., Kramer M., Lyne A. G., Manchester R. N., McLaughlin M. A., Stairs I. H., Hobbs G., Possenti A., Lorimer D. R., D’Amico N., Camilo F., Burgay M., 2005, *ApJ Lett*, 618, L119
- Flanagan E. E., Hughes S. A., 1998, *Phys. Rev.*, D57, 4535
- Flannery B. P., van den Heuvel E. P. J., 1975, *A&A*, 39, 61
- Fryer C. L., Woosley S. E., Hartmann D. H., 1999, *ApJ*, 526, 152
- Geppert U., Urpin V., 1994, *MNRAS*, 271, 490
- Gnusareva V. S., Lipunov V. M., 1985, *Soviet Astronomy*, 29, 645
- Gondek-Rosińska D., Bejger M., Bulik T., Gourgoulhon E., Haensel P., Limousin F., Taniguchi K., Zdunik L., 2007, *Advances in Space Research*, 39, 271
- Gondek-Rosińska D., Bulik T., Belczyński K., 2005a, *Memorie della Societa Astronomica Italiana*, 76, 632
- Gondek-Rosińska D., Bulik T., Belczyński K., 2005b, *Memorie della Societa Astronomica Italiana*, 76, 513
- Gondek-Rosińska D., Bulik T., Belczyński K., 2007, *Advances in Space Research*, 39, 285
- Gonthier P. L., Ouellette M. S., Berrier J., O’Brien S., Harding A. K., 2002, *ApJ*, 565, 482
- Gonthier P. L., Roberts J. J., Nagelkirk E., Stam M., Harding A. K., 2010, in *Bulletin of the American Astronomical Society Vol. 42 of Bulletin of the American Astronomical Society, Population Synthesis of Radio and Gamma-ray Pulsars in the Fermi Era.* pp 680+
- Gonthier P. L., Van Guilder R., Harding A. K., 2004, *ApJ*, 604, 775
- Gunn J. E., Ostriker J. P., 1970, *ApJ*, 160, 979
- Hartman J. W., Bhattacharya D., Wijers R., Verbunt F., 1997, *A&A*, 322, 477
- Hobbs G., Lorimer D. R., Lyne A. G., Kramer M., 2005, *MNRAS*, 360, 974
- Hulse R. A., Taylor J. H., 1975, *ApJ Lett*, 195, L51
- Hurley J. R., Pols O. R., Tout C. A., 2000, *Mon. Not. Roy. Astron. Soc.*, 315, 543
- Illarionov A. F., Sunyaev R. A., 1975, *Astron. Astrophys.*, 39, 185
- Jacoby B. A., Cameron P. B., Jenet F. A., Anderson S. B., Murty R. N., Kulkarni S. R., 2006, *ApJ Lett*, 644, L113
- Jahan-Miri M., 2000, *ApJ*, 532, 514
- Janssen G. H., Stappers B. W., Kramer M., Nice D. J., Jessner A., Cognard I., Purver M. B., 2008, *A&A*, 490, 753
- Jorgensen H., Lipunov V. M., Panchenko I. E., Postnov K. A., Prokhorov M. E., 1995, *ApSS*, 231, 389
- Kalogera V., Narayan R., Spergel D. N., Taylor J. H., 2001, *ApJ*, 556, 340
- Kasian L., 2008, in *Bassa C. G. Wang Z. C. A., M. K. V.,*

- eds, 40 Years of Pulsars: Millisecond Pulsars, Magnetars and More Vol. 983 of American Institute of Physics Conference Series, Timing and Precession of the Young, Relativistic Binary Pulsar PSR J1906+0746. pp 485–487
- Kiel P. D., Hurley J. R., 2009, *MNRAS*, 395, 2326
- Kiel P. D., Hurley J. R., Bailes M., Murray J. R., 2008, *MNRAS*, 388, 393
- Konar S., Bhattacharya D., 1997, *MNRAS*, 284, 311
- Konar S., Bhattacharya D., 1999a, *MNRAS*, 303, 588
- Konar S., Bhattacharya D., 1999b, *MNRAS*, 308, 795
- Konar S., Choudhuri A. R., 2004, *MNRAS*, 348, 661
- Kuiper G. P., 1935, *PASP*, 47, 15
- Kulczycki K., Bulik T., Belczyński K., Rudak B., 2006, *A&A*, 459, 1001
- Large M. I., 1971, in Davies R. D., Graham-Smith F., eds, *The Crab Nebula Vol. 46 of IAU Symposium, The Galactic Population of Pulsars*. Reidel, Dordrecht, pp 165–+
- Lipunov V. M., Postnov K. A., Prokhorov M. E., Panchenko I. E., Jorgensen H. E., 1995, *ApJ*, 454, 593
- Lorimer D. R., 2008, *Living Reviews in Relativity*, 11, 8
- Lorimer D. R., Kramer M., 2004, *Handbook of Pulsar Astronomy*. Cambridge University Press
- Lovelace R. V. E., Romanova M. M., Bisnovatyi-Kogan G. S., 2005, *ApJ*, 625, 957
- Lyne A. G., Burgay M., Kramer M., Possenti A., Manchester R. N., Camilo F., McLaughlin M. A., Lorimer D. R., D’Amico N., Joshi B. C., Reynolds J., Freire P. C. C., 2004, *Science*, 303, 1153
- Lyne A. G., Manchester R. N., 1988, *MNRAS*, 234, 477
- Lyne A. G., Manchester R. N., Taylor J. H., 1985, *MNRAS*, 213, 613
- Lyutikov M., Thompson C., 2005, *ApJ*, 634, 1223
- Manchester R. N., Hobbs G. B., Teoh A., Hobbs M., 2005, *VizieR Online Data Catalog*, 7245, 0
- Manchester R. N., Lyne A. G., Camilo F., Bell J. F., Kaspi V. M., D’Amico N., McKay N. P. F., Crawford F., Stairs I. H., Possenti A., Kramer M., Sheppard D. C., 2001, *MNRAS*, 328, 17
- Maron O., Kijak J., Kramer M., Wielebinski R., 2000, *A&AS*, 147, 195
- Melatos A., Phinney E. S., 2001, *Publ. Astron. Soc. Aust.*, 18, 421
- Miyamoto M., Nagai R., 1975, *PASJ*, 27, 533
- Muslimov A. G., Tsygan A. I., 1985, *ApSS*, 115, 43
- Narayan R., Ostriker J. P., 1990, *ApJ*, 352, 222
- Ostriker J. P., Gunn J. E., 1969, *ApJ*, 157, 1395
- Paczynski B., 1990, *ApJ*, 348, 485
- Perera B. B. P., McLaughlin M. A., Kramer M., Stairs I. H., Ferdman R. D., Freire P. C. C., Possenti A., Breton R. P., Manchester R. N., Burgay M., Lyne A. G., Camilo F., 2010, *ApJ*, 721, 1193
- Peters P. C., 1964, *Phys. Rev.*, 136, B1224
- Phinney E. S., Sigurdsson S., 1991, *Nature*, 349, 220
- Piran T., 1992, in R. S. J., ed., *American Institute of Physics Conference Series Vol. 272 of American Institute of Physics Conference Series, γ -ray bursts and neutron star mergers-possibly the strongest explosions in the universe*. pp 1626–1633
- Popov S. B., Colpi M., Treves A., Turolla R., Lipunov V. M., Prokhorov M. E., 2000, *Astronomical and Astrophysical Transactions*, 19, 471
- Portegies Zwart S. F., Yungelson L. R., 1998, *A&A*, 332, 173
- Quinn T., Perrine R. P., Richardson D. C., Barnes R., 2010, *AJ*, 139, 803
- Ransom S. M., Cordes J. M., Eikenberry S. S., 2003, *ApJ*, 589, 911
- Romani R. W., 1990, *Nature*, 347, 741
- Romanova M. M., Ustyugova G. V., Koldoba A. V., Lovelace R. V. E., 2004, *ApJ Lett*, 616, L151
- Rudak B., Ritter H., 1994, *MNRAS*, 267, 513
- Ruderman M., 1991a, *ApJ*, 366, 261
- Ruderman M., 1991b, *ApJ*, 382, 587
- Ruderman R., 1991c, *ApJ*, 382, 576
- Scalo J. M., 1986, *Fundamentals of Cosmic Physics*, 11, 1
- Shibazaki N., Murakami T., Shaham J., Nomoto K., 1989, *Nature*, 342, 656
- Stairs I. H., 2004, *Science*, 304, 547
- Stollman G. M., 1987, *A&A*, 178, 143
- Story S. A., Gonthier P. L., Harding A. K., 2007, *ApJ*, 671, 713
- Taam R. E., van den Heuvel E. P. J., 1986, *ApJ*, 305, 235
- Tauris T. M., Manchester R. N., 1998, *MNRAS*, 298, 625
- Taylor J. H., Manchester R. N., 1977, *ApJ*, 215, 885
- Timmes F. X., Woosley S. E., Weaver T. A., 1996, *ApJ*, 457, 834
- Urpin V., Geppert U., 1995, *MNRAS*, 275, 1117
- Urpin V., Konenkov D., Urpin V., 1997, *MNRAS*, 292, 167
- Vanbeveren D., De Loore C., Van Rensbergen W., 1998, *AAPR*, 9, 63
- Weaver T. A., Woosley S. E., 1993, *Phys. Rep.*, 227, 65
- Webbink R. F., 1984, *ApJ*, 277, 355
- Weisberg J. M., Taylor J. H., 2005, in Rasio F. A., Stairs I. H., eds, *Binary Radio Pulsars Vol. 328 of Astronomical Society of the Pacific Conference Series, The Relativistic Binary Pulsar B1913+16: Thirty Years of Observations and Analysis*. pp 25–+
- Woosley S. E., 1986, in Audouze J., Chiosi C., Woosley S. E., eds, *Saas-Fee Advanced Course 16: Nucleosynthesis and Chemical Evolution Nucleosynthesis and Stellar Evolution*. Geneva Observatory, CH-190 Sauverny, pp 1–+
- Young M. D., Manchester R. N., Johnston S., 1999, *Nature*, 400, 848
- Zhang C. M., Kojima Y., 2006, *MNRAS*, 366, 137

